iScience

CellPress

Article

The Phosphoinositide Kinase PIKfyve Promotes Cathepsin-S-Mediated Major Histocompatibility Complex Class II Antigen Presentation

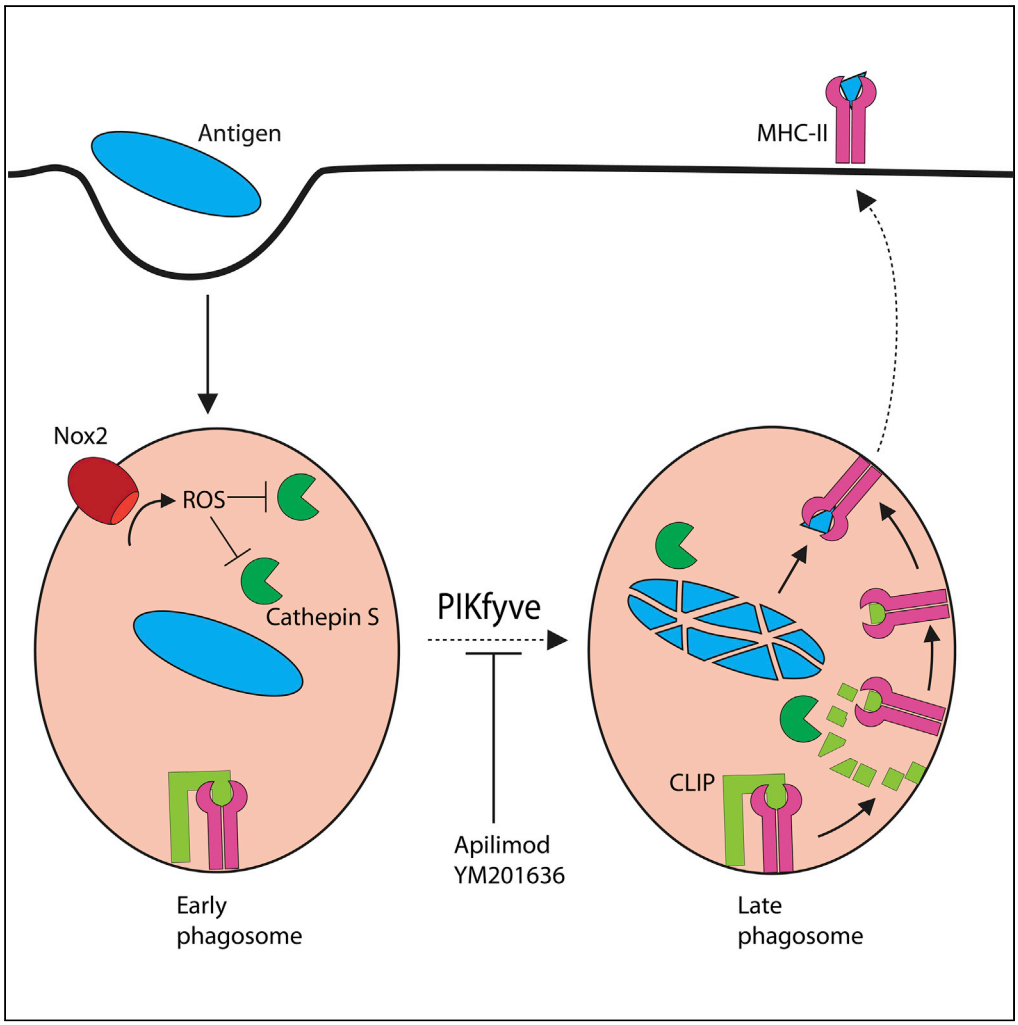

Maksim V. Baranov, Frans Bianchi, Anastasiya Schirmacher, ..., Carolyn R. Bertozzi, Ulf Diederichsen, Geert van den Bogaart

g.van.den.bogaart@rug.nl

HIGHLIGHTS

PIKfyve converts PI(3)P into PI(3,5)P_2 on the surface of endosomes and phagosomes

PIKfyve of DCs modulates phagosomal maturation, acidification, and ROS production

PIKfyve defects disrupt cathepsin S trafficking and activity

Inactive cathepin S slows Ii processing for MHC class II trafficking and antigen loading

Baranov et al., iScience *11*, 160–177
January 25, 2019
https://doi.org/10.1016/j.isci.2018.12.015

iScience

CellPress

Article

The Phosphoinositide Kinase PIKfyve Promotes Cathepsin-S-Mediated Major Histocompatibility Complex Class II Antigen Presentation

Maksim V. Baranov,[1] Frans Bianchi,[1,3] Anastasiya Schirmacher,[2] Melissa A.C. van Aart,[1] Sjors Maassen,[1,3] Elke M. Muntjewerff,[1] Ilse Dingjan,[1] Martin ter Beest,[1] Martijn Verdoes,[1] Samantha G.L. Keyser,[4] Carolyn R. Bertozzi,[5] Ulf Diederichsen,[2] and Geert van den Bogaart[1,3,6,*]

SUMMARY

Antigen presentation to T cells in major histocompatibility complex class II (MHC class II) requires the conversion of early endo/phagosomes into lysosomes by a process called maturation. Maturation is driven by the phosphoinositide kinase PIKfyve. Blocking PIKfyve activity by small molecule inhibitors caused a delay in the conversion of phagosomes into lysosomes and in phagosomal acidification, whereas production of reactive oxygen species (ROS) increased. Elevated ROS resulted in reduced activity of cathepsin S and B, but not X, causing a proteolytic defect of MHC class II chaperone invariant chain Ii processing. We developed a novel universal MHC class II presentation assay based on a bio-orthogonal "clickable" antigen and showed that MHC class II presentation was disrupted by the inhibition of PIKfyve, which in turn resulted in reduced activation of $CD4^+$ T cells. Our results demonstrate a key role of PIKfyve in the processing and presentation of antigens, which should be taken into consideration when targeting PIKfyve in autoimmune disease and cancer.

INTRODUCTION

Endocytosis and phagocytosis of microbial pathogens, virus-infected cells, and cancer cells is essential for their immune clearance by phagocytes of the immune system (Fairn and Grinstein, 2012; Neefjes et al., 2017). In addition, dendritic cells present peptides derived from ingested antigens on major histocompatibility complex (MHC) classes I and II to T lymphocytes and are thereby responsible for the initiation of adaptive immune responses (Banchereau and Steinman, 1998). There are various types of endocytosis and phagocytosis, which differ in the receptors engaged, the role of the cytoskeleton, cage proteins, and lipid composition (Fairn and Grinstein, 2012; Levin et al., 2015; Nunes et al., 2013). Following uptake, endosomes and phagosomes undergo a transition from early to late endo/phagosomes and eventually to lysosomes. This process is mediated by membrane remodeling called maturation, where endosomes and phagosomes fuse with other endosomes and lysosomes and recruit cytosolic proteins to their membranes, such as Rab-GTPases and tethering factors (Egami, 2016; Fairn and Grinstein, 2012; Flannagan et al., 2012; Naufer et al., 2018; Neefjes et al., 2017; Uribe-Querol and Rosales, 2017; Vieira et al., 2003). Early endosomes and phagosomes are only mildly acidic or even basic (Flannagan et al., 2009; Mantegazza et al., 2008; Savina et al., 2006), whereas lysosomes and phagolysosomes are very acidic due to activation of vacuolar proton pumps (pH < 5; Trombetta et al., 2003) and have increased presence and activity of metabolic enzymes for the degradation of ingested material (Kinchen and Ravichandran, 2008).

The MHC class II loading of proteolytically derived peptides occurs within specialized lysosome-like compartments called MHC class II compartments (MIIC) (Amigorena et al., 1994; Calafat et al., 1994; Castellino and Germain, 1995; Sadegh-Nasseri, 2016; Tulp et al., 1994; West et al., 1994). Within these acidic luminal compartments, the non-polymorphic chain of MHC class II Ii is proteolytically activated by its cleavage, reducing it to the 24-amino acid class II-associated Ii peptide (CLIP) (Jasanoff et al., 1999). Ii is a chaperone carrying sorting signals on its cytoplasmic tail and interacting with MHC class II thereby controlling its trafficking from the endoplasmic reticulum to the *trans*-Golgi network (TGN), endosomal compartments, and eventually to the cell surface (Jones et al., 1978; Teyton et al., 1990). Ii prevents premature antigen loading into the cleft of MHC class II, whereas CLIP can be exchanged in MIIC for an antigen peptide by the chaperone human leukocyte antigen (HLA)-DM. The protease cathepsin S (CatS) plays an essential role for Ii processing to CLIP and for the proteolytic processing of ingested antigen (Honey and Rudensky, 2003; Riese

[1]Department of Tumor Immunology, Radboud University Medical Center, Radboud Institute for Molecular Life Sciences, Geert Grooteplein 28, 6525GA Nijmegen, the Netherlands

[2]Institute of Organic and Biomolecular Chemistry, Georg-August-University of Göttingen, Tammannstr. 2, 37077 Göttingen, Germany

[3]Department of Molecular Immunology, Groningen Biomolecular Sciences and Biotechnology Institute, University of Groningen, Nijenborgh 7, Groningen 9747 AG, the Netherlands

[4]Department of Chemistry, University of California, Berkeley, CA 94720, USA

[5]Department of Chemistry and Howard Hughes Medical Institute, Stanford University, Stanford, CA 94305, USA

[6]Lead Contact

*Correspondence: g.van.den.bogaart@rug.nl

https://doi.org/10.1016/j.isci.2018.12.015

et al., 1996; Villadangos and Ploegh, 2000), and only three cathepsins (CatB, CatH, and CatS) suffice for generating essential immunodominant epitopes *in vitro* (Kim et al., 2014a).

A central hallmark of endo/phagosomal maturation is the progressive change in the content of phosphoinositide lipids on the endosomal and phagosomal membrane (Levin et al., 2015; Shisheva, 2001). These phosphoinositides are important for endo/phagosomal maturation, as they are major determinants of organellar identity and form anchor points for numerous proteins involved in membrane trafficking or cytoskeletal tethering (Baranov et al., 2016, 2017; Levin et al., 2015). Within minutes after uptake, phosphatidylinositol 4,5-bisphosphate, which is the main phosphoinositide species at the plasma membrane, is converted into phosphatidylinositol 3-phosphate (PI(3)P) by various kinases and phosphatases. PI(3)P is the main phosphoinositide species at early endosomes and phagosomes and resides there for 5–10 min (Ellson et al., 2001a; Fratti et al., 2001; Gillooly et al., 2000; Vieira et al., 2003) before the acidification of these organelles (Naufer et al., 2018). The maturation of early into late endo/phagosomes and lysosomes requires the conversion of PI(3)P into phosphatidylinositol 3,5-bisphosphate ($PI(3,5)P_2$) (Ho et al., 2012; Sbrissa et al., 2002). $PI(3,5)P_2$ is a low-abundance phosphoinositide amounting to ~0.04%–0.1% of the total phosphoinositide pool (Ho et al., 2012; McCartney et al., 2014). Phosphoinositide 5-kinase (PIKfyve; yeast ortholog Fab1p) is the sole enzyme capable of producing $PI(3,5)P_2$ from PI(3)P, which it targets via its FYVE domain (Ho et al., 2012; Sbrissa et al., 2002; Shisheva et al., 2015). Blocking of PIKfyve activity delays phagosomal maturation, leading to the buildup of cellular PI(3)P and a drastic reduction of cellular levels of $PI(3,5)P_2$ (Hazeki et al., 2012; Kim et al., 2014b). Given the late endosome/lysosome-like nature of MIIC, a role of $PI(3,5)P_2$ and PIKfyve in MHC class II presentation can be expected, but has not been shown.

PIKfyve can be inhibited by two small molecule inhibitors: apilimod (STA-5,326) (Cai et al., 2013) and YM201636 (Hazeki et al., 2012; Jefferies et al., 2008). Apilimod was originally developed to treat inflammatory diseases (Burakoff et al., 2006; Krausz et al., 2012; Sands et al., 2010; Wada et al., 2007, 2012) and was later found to specifically target and inhibit PIKfyve (Cai et al., 2013). YM201636 is a specific antagonist of PIKfyve (Jefferies et al., 2008), and although it has not been tested in clinical trials, it is commonly used to inhibit PIKfyve (Compton et al., 2016; Gomez et al., 2018; Hazeki et al., 2012; Ikonomov et al., 2009; Kerr et al., 2010; Kim et al., 2014b; Krishna et al., 2016; Sbrissa et al., 2012). Pharmacological inhibition of PIKfyve or expression of a dominant negative form of PIKfyve (Ikonomov et al., 2001; Jefferies et al., 2008; Shisheva, 2001) causes the formation of enlarged ("foam-like") vacuoles (Cai et al., 2013; Dong et al., 2010; Jefferies et al., 2008; Min et al., 2014), likely because of osmotic differences caused by the reduced activity of $PI(3,5)P_2$-dependent cation channels such as the lysosomal cation channel TRPML1/MCOLN1 (Compton et al., 2016). These enlarged vacuoles are likely endosomes that cannot be reformed into lysosomes (Bissig et al., 2017), and their formation can be used as a readout of depletion of cellular $PI(3,5)P_2$ (Kim et al., 2014b).

Given the role of late endosome/lysosome-related MIIC in the proteolytic processing of antigen and subsequent MHC class II loading, we hypothesized that interfering with PIKfyve activity would inhibit the degradation and presentation of antigen by dendritic cells. To address this hypothesis, we studied the effects of PIKfyve inhibition by apilimod and YM201636 on endo/phagosomal maturation, protease activity, and antigen presentation. As reported (Cai et al., 2013, 2014), PIKfyve inhibition blocked interleukin (IL)-12 secretion in monocyte-derived dendritic cells. PIKfyve inhibition also affected the maturation of phagosomes, with impaired acidification and lower recruitment of the lysosomal proteins lysosome-associated membrane protein 1 (LAMP1) and mannose 6-phosphate receptor (M6PR) to phagosomes, whereas the early phagosomal markers PI(3)P and EEA1 were more abundant (Compton et al., 2016; Dayam et al., 2017; Dove et al., 2009; Gayle et al., 2017a; Gomez et al., 2018; Hazeki et al., 2012; Ikonomov et al., 2009; Kerr et al., 2010; Kim et al., 2014b; Krishna et al., 2016; Sbrissa et al., 2007, 2012). Moreover, inhibition of PIKfyve selectively blocked the activity of cathepsin B and S, and this resulted in an increased presence of Ii-bound MHC class II within the cell, but not on the cell surface. PIKfyve inhibitors caused prolonged presence of the NADPH oxidase NOX2, which is present on early, but not late, endosomes and phagosomes (Dingjan et al., 2017a, 2017b). This resulted in increased reactive oxygen species (ROS) production, leading to lower activity of CatS. We show that the impaired processing of Ii and MHC class II trafficking defects upon blockage of endo/phagosomal maturation with PIKfyve inhibitors results in lower MHC class II antigen presentation. This was demonstrated with a novel assay based on a viral antigen carrying an unnatural amino acid amendable to bio-orthogonal labeling of the MHC-class-II-presented epitope. The combined effects of reduced proteolytic processing and reduced MHC class II presentation upon blocking PIKfyve

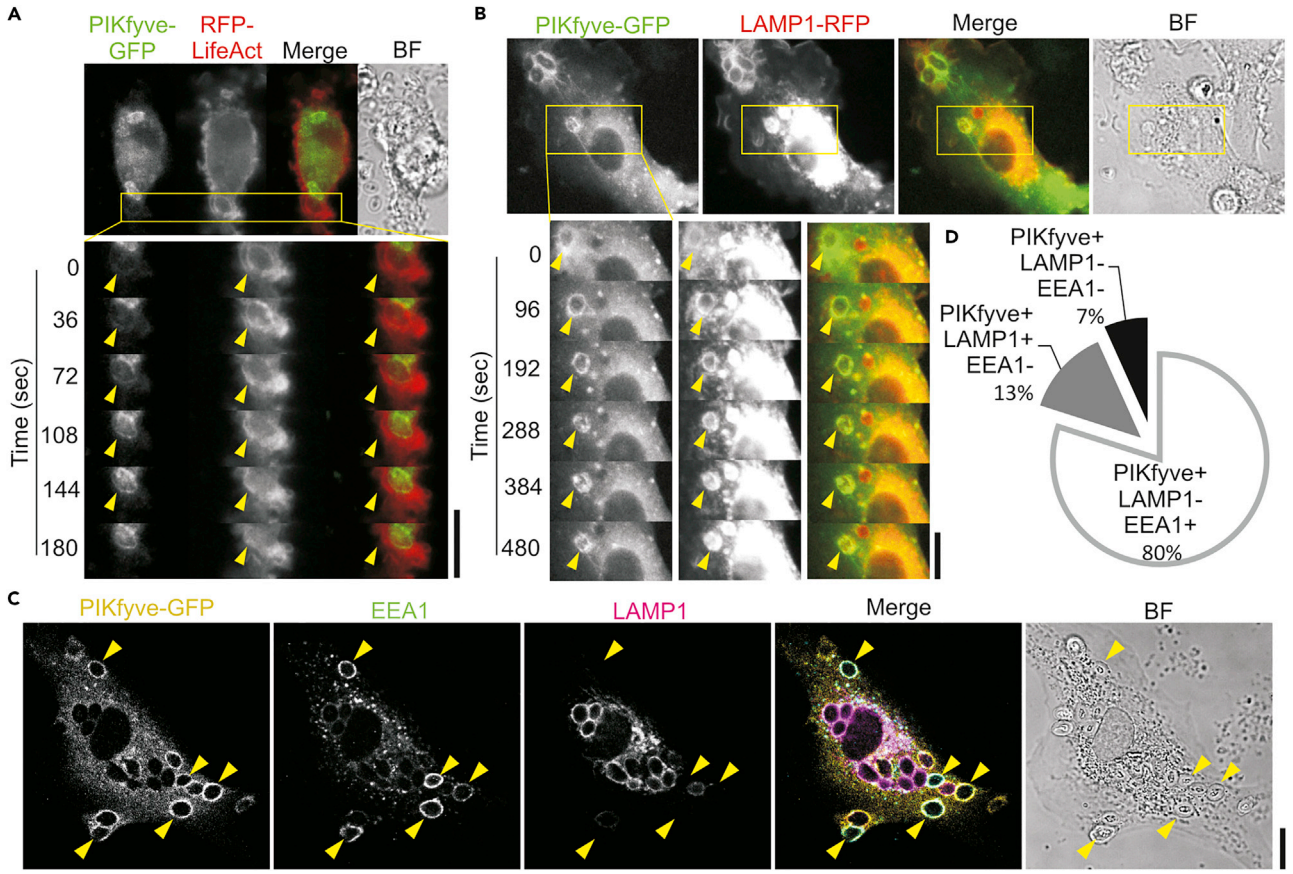

Figure 1. PIKfyve Is Present Early during Phagosomal Maturation

(A) Live cell imaging of a human monocyte-derived dendritic cell overexpressing human PIKfyve-GFP (green in merge) together with the F-actin-binding probe RFP-LifeAct (red) and pulsed with IgG-opsonized zymosan particles. The insets show snapshots at the indicated time points. Yellow arrowheads, time series of phagosome. See also Video S1. BF, brightfield.

(B) Same as (A), but now with PIKfyve-GFP (green) and LAMP1-RFP (red). See also Video S2.

(C) Confocal micrograph of representative zymosan-pulsed (1 hr) dendritic cell overexpressing PIKfyve-GFP (yellow in merge) with immunostaining for EEA1 (green) and LAMP1 (magenta). Yellow arrowheads, PIKfyve-GFP and EEA1 double-positive phagosomes.

(D) Quantification of (C) (~150 phagosomes per donor; three donors).

Scale bars, 10 μm. See also Figure S1.

result in an impaired activation of antigen-specific T cells. These results show a key role for PIKfyve in T cell activation, and this should be taken into consideration for the use of PIKfyve-targeting drugs in clinical trials.

RESULTS

PIKfyve Inhibition Delays Phagosomal Maturation

We started by determining whether PIKfyve would localize to antigen-containing compartments. To visualize the localization of PIKfyve in live cells, we transfected dendritic cells differentiated from human-blood-derived monocytes with plasmids coding for GFP-tagged PIKfyve (PIKfyve-GFP) (Figure 1A; Video S1). The actin cytoskeleton was visualized by simultaneous transfection with a plasmid coding for the F-actin-binding probe LifeAct fused to the red-shifted fluorescent protein mRFPruby (Riedl et al., 2008). Late endo/phagosomes and lysosomes were identified with LAMP1 fused to red fluorescent protein (RFP) (Figure 1B; Video S2) (Sherer et al., 2003). The dendritic cells were pulsed with the model pathogen zymosan, relatively large yeast-derived particles (~4–5 μm diameter) that allow for the unequivocal assignment of phagosomal localization of candidate proteins by microscopy and result in an increased expression of PIKfyve (Figure S1A). We observed that PIKfyve-GFP was recruited within 2 min after the formation of the phagosomal F-actin cytoskeleton (Figure 1A), which we recently showed is formed at the nascent cup of emerging

phagosomes by tethering to phosphatidylinositol 3,4-bisphosphate ($PI(3,4)P_2$) and is subsequently removed after closure of the phagocytic cup (Baranov et al., 2016). At later time points after uptake (>7 min), the signal of PIKfyve-GFP gradually decreased at the phagosomes, whereas the signal of LAMP1-RFP increased (Figure 1B). We also immunostained zymosan-pulsed dendritic cells expressing PIKfyve-GFP for endogenous LAMP1 as well as for the early endosomal marker EEA1 (Figure 1C). EEA1 is known to bind to early endo/phagosomes by interactions of its FYVE domain with PI(3)P (Ho et al., 2012; Sbrissa et al., 2002), which is the substrate for PIKfyve. PIKfyve-GFP was partially co-residing with EEA1 on phagosomes, whereas overlap with LAMP1 was lower (Figure 1D). Together, these results show that PIKfyve is recruited to phagosomes within minutes after their formation and remains present at early phagosomes before their conversion into late phagosomes.

Next, we validated the reported inhibition of endosome and phagosome maturation by blockage of PIKfyve activity with apilimod and YM201636 (Compton et al., 2016; Dayam et al., 2017; Dove et al., 2009; Gayle et al., 2017a; Gomez et al., 2018; Hazeki et al., 2012; Ikonomov et al., 2009; Kerr et al., 2010; Kim et al., 2014b; Krishna et al., 2016; Sbrissa et al., 2007, 2012). We selected concentrations of 200 nM apilimod (Cai et al., 2013; Compton et al., 2016; Terajima et al., 2016; Wada et al., 2012; Wong et al., 2017) and 4 μM YM201636 (Currinn et al., 2016; Ikonomov et al., 2009), which did not significantly affect the viability of the dendritic cells, although metabolic activity was somewhat affected by apilimod (by the MTT (3-(4,5-dimethylthiazol-2-yl)-2,5-diphenyltetrazolium bromide) assay; Baranov et al., 2016; Baranov et al., 2017; Dingjan et al., 2016) and YM201636 treatment non-significantly increased the fraction of early apoptotic cells (by annexin V staining; Figures S1B–S1D). These concentrations were used in previous studies and resulted in inhibition of IL-12 production by the dendritic cells (Cai et al., 2013; Wada et al., 2012) (Figure S1E). Treatment of dendritic cells with apilimod or YM201636 resulted in massive cellular vacuolization (Figure S1F), a well-known effect of PIKfyve inhibition (Cai et al., 2013; Dayam et al., 2017; Krishna et al., 2016). This vacuolization was also observed when a dominant negative form of PIKfyve was expressed (PIKfyve-GFP with K1831E [Cai et al., 2013; Ikonomov et al., 2001; Sbrissa et al., 2000]) (Figure S1G) and with small interfering RNA (siRNA) knockdown (Figure S1H). Moreover, treatment of dendritic cells by apilimod or YM201636 compromised phagocytosis of the zymosan particles as well as endocytosis of fluorescently labeled albumin by almost half (Figures S1I and S1J). Previously reported PIKfyve perturbations led to inhibition of IgG-latex bead uptake by neutrophils (Dayam et al., 2017) and mouse RAW 264.7 macrophages (Kim et al., 2014b) and to lower *Escherichia coli* uptake by RAW 264.7 macrophages (Wong et al., 2017). To account for this reduced antigen uptake, we present our results relative to the total number of phagosomes per cell. Both apilimod and YM201636 treatment resulted in blockage of phagosome maturation, as apparent from a reduced fraction of LAMP1 and increased fractions of EEA1-positive (Figures 2A and 2B) and PI(3)P-positive phagosomes (Figures 2C and 2D). In addition, phagosomal recruitment of M6PR, another late endosomal marker that is involved in trafficking from the TGN to lysosomes, was also reduced upon apilimod and YM201636 treatment (Figures S1K and S1L). To exclude off-target effects of the drugs, we performed siRNA knockdown of PIKfyve. Even though we only reached an ~50% knockdown efficiency of PIKfyve by qPCR (Figure S1M), this led to a reduced recruitment of LAMP1 to phagosomes (Figure S1N) similar to the small molecule inhibitors. Finally, acidification of the phagosomal lumen was reduced by apilimod or YM201636 treatment, as shown by experiments with zymosan conjugated to pHRodo, a pH-sensitive dye with increased fluorescence at low pH (Figures 2E and 2F). Similar blockage of acidification was observed with PIKfyve siRNA knockdown (Figure 2G).

Cathepsin B and S Activities and Proteolytic Activation of MHC Class II Are Reduced upon PIKfyve Inhibition

Phagosomal maturation and acidification are necessary to trigger the activity of hydrolases involved in the degradation of ingested antigen, and thereby for deriving antigenic peptides for presentation in MHC class II (Blum et al., 2013; ten Broeke et al., 2013). A major class of proteases are cysteine cathepsins, named after the catalytic cysteine located within their active sites (Verma et al., 2016) and consisting of 11 family members present in endosomes, phagosomes, and lysosomes (Turk et al., 2012). CatS is predominantly expressed by professional antigen-presenting cells, such as dendritic cells and B cells (Blum et al., 2013) and, unlike other cathepsins, is active not only in acidic but also in neutral and slightly alkaline environments (Jancic et al., 2007; Kirschke et al., 1989). As we observed that inhibition of PIKfyve by apilimod or YM201636 impaired lysosomal acidification and affected trafficking to late endosomes/lysosomes, we hypothesized that this would alter the activity of cathepsins. We applied the activity-based probe BMV109 to living cells before lysis (Verdoes et al., 2013). The BMV109 probe results in covalent attachment of a fluorophore to the catalytic sites of active cysteine cathepsins (Verdoes et al., 2013), thereby allowing for the quantitative assessment of their activities by in-gel fluorescence (Figure S2A). We compared unstimulated

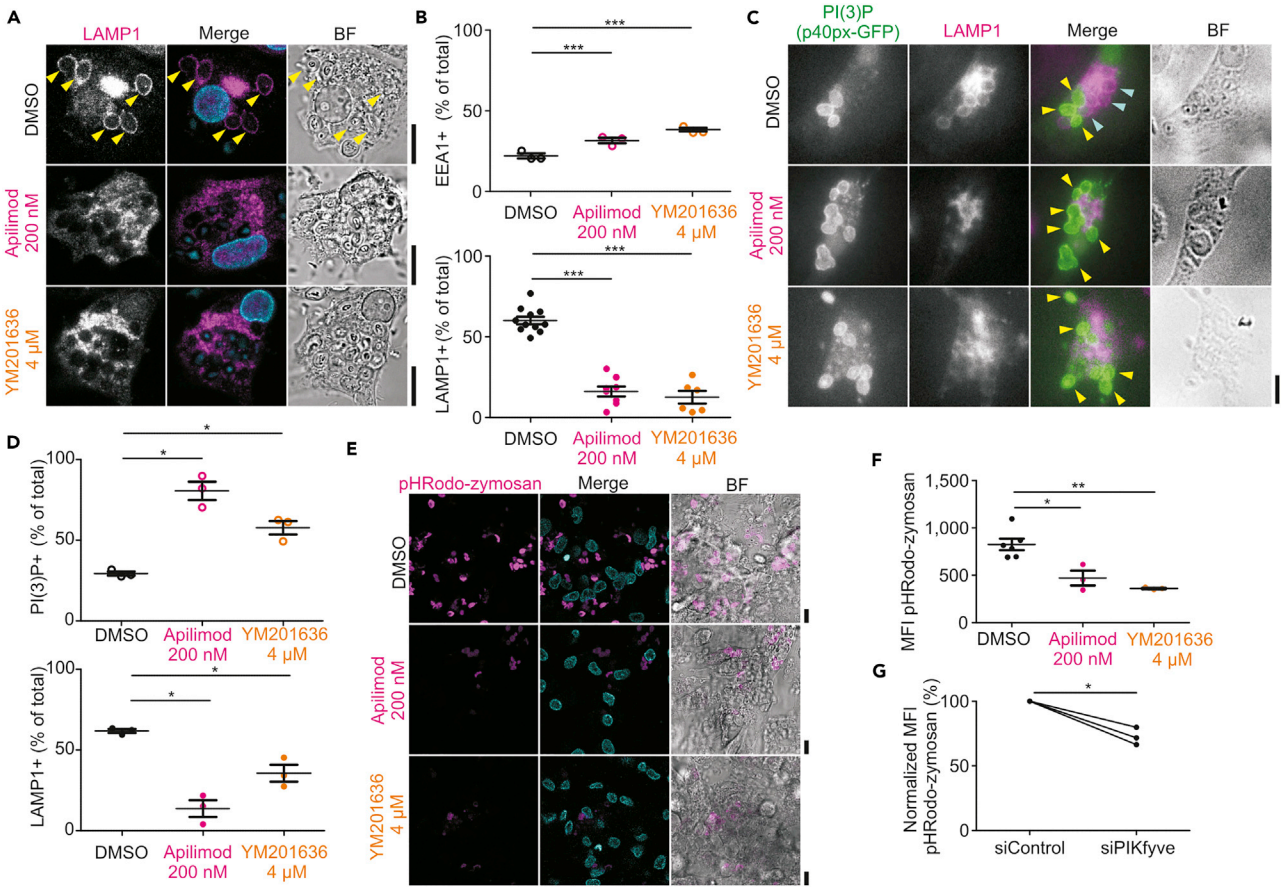

Figure 2. PIKfyve Controls Phagosomal Maturation

(A) Confocal images of representative dendritic cells treated with apilimod (200 nM) or YM201636 (4 μM) for 3 hr and pulsed with zymosan 1 hr before fixation. DMSO, vehicle control. Cells were immunolabeled for LAMP1 (magenta in merge). Blue, DAPI staining. BF, brightfield.

(B) Quantification of (A) normalized to the total number of phagosomes per cell (~150 phagosomes per condition per donor; mean ± SEM of three donors for EEA1 and six donors for LAMP1).

(C) Epifluorescence microscopy of representative dendritic cells expressing GFP-tagged phosphoinositide-probe for PI(3)P based on PX domain of NCF4 (PI(3)P; green in merge) and immunolabeled for LAMP1 (magenta). The cells were treated as in (A). Yellow arrowheads, PI(3)P-positive phagosomes; cyan arrowheads, LAMP1-positive phagosomes.

(D) Quantification of (C) normalized to the total number of phagosomes per cell (~116 phagosomes per condition per donor; mean ± SEM of three donors).

(E) Confocal imaging of dendritic cells treated with DMSO, apilimod, or YM201636 for 3 hr before addition of pHRodo-labeled zymosan 1 hr before live imaging. The color intensity of pHRodo (magenta) scales with acidic pH. Cyan in merge, Hoechst.

(F) Quantification of (E); MFI, mean fluorescence intensity (mean ± SEM for three donors, ~1,000 phagosomes per condition per donor).

(G) Same as (F), but now with siPIKfyve (~400 phagosomes per condition per donor; see also Figure S1M for knockdown levels).

Scale bars: 10 μm. *P < 0.05, **P < 0.01, ***P < 0.001. See also Figure S1.

and zymosan-pulsed dendritic cells treated with apilimod or YM201636 (Figure 3A). Analysis of protein levels by western blot showed that PIKfyve inhibitors did not cause changes of total cathepsin levels (Figure S2A). For unstimulated cells, we observed reduced cathepsin B and S activities by treatment with apilimod or YM201636, whereas the activity of cathepsin X was not altered (Figures 3B, 3C, and S2B). However, stimulation of the cells with zymosan diminished these effects, and significant differences in cathepsin activity could no longer be detected after 1-hr incubation. Immunolabeling of endogenous CatS in phagocytic dendritic cells was visible at the core of the zymosan particles (Figure 3D). Microscopy experiments with the activity-based probe BMV109 confirmed that this is the site of cathepsin activity (Figures S2C and S2D). BMV109 signal became apparent at phagosomes 30–60 min after zymosan uptake and was present in LAMP1-positive phagosomes (Figure S2C). Immunofluorescence microscopy revealed that the majority of CatS-positive phagosomes are also LAMP1 positive (Figure S2E). Treatment with apilimod or YM201636 reduced the signals of both CatS immunostaining (Figures 3D–3E) and BMV109 (Figures S2D

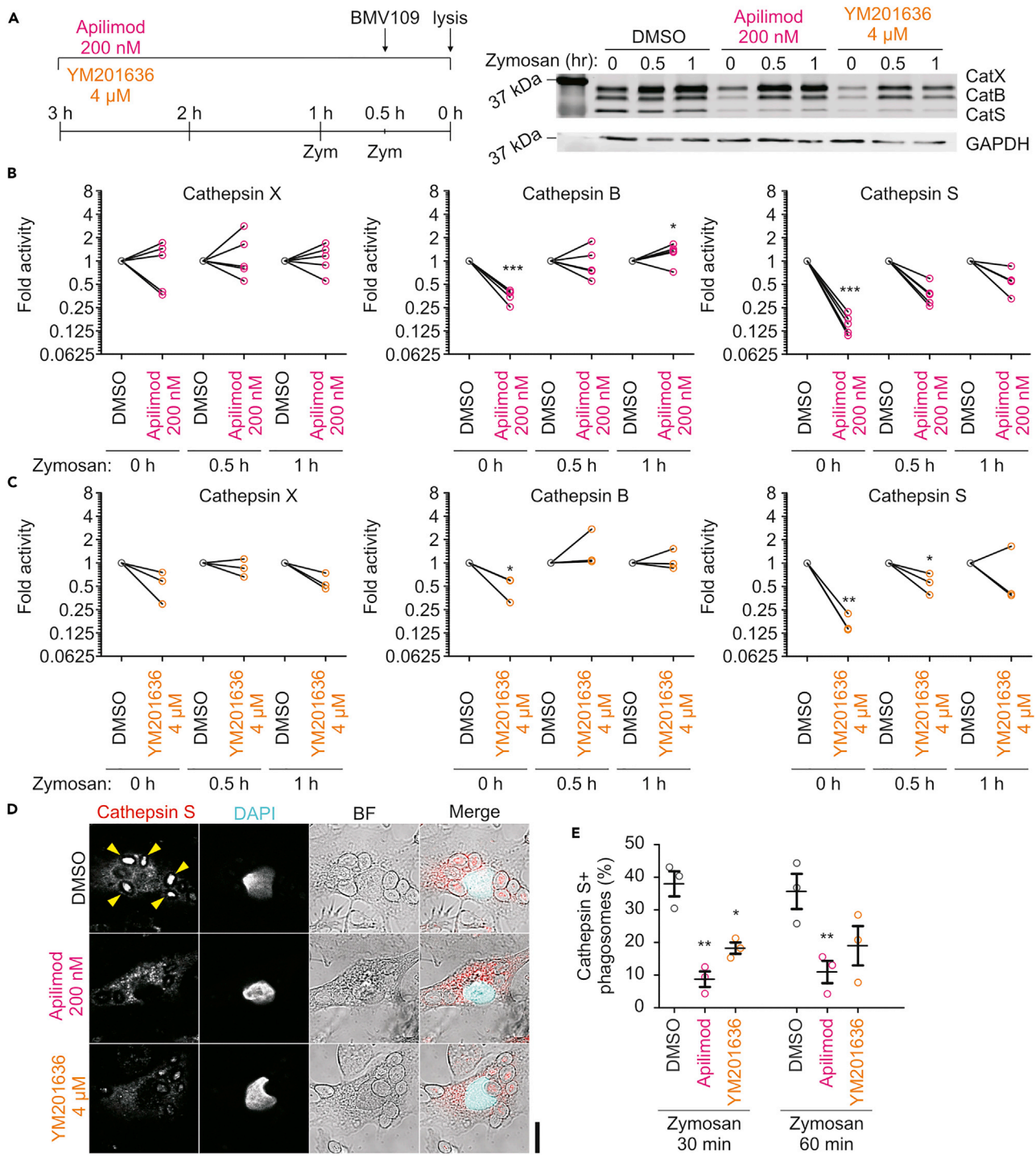

Figure 3. Pharmacological Inhibition of PIKfyve Blocks Cathepsin S Activity and Trafficking

(A) SDS-PAGE with in-gel fluorescence of the BMV109-Cy5 activity-based probe labeling cathepsin X (CatX; top band), cathepsin B (CatB; middle band), and cathepsin S (CatS; lower band) in resting dendritic cells (0 hr) or after stimulation with zymosan for 0.5 or 1 hr. Cells were treated with DMSO (vehicle control), apilimod, or YM201636 for 3 hr before lysis according to the left-hand scheme. GAPDH, loading control by western blot. Only part of the SDS PAGE/polyvinylidene fluoride blot is shown; the rest of the image carried no information.

(B and C) Quantification of (A) (individual donors shown; normalized to DMSO controls).

Figure 3. *Continued*

(D) Confocal images of representative dendritic cells treated with PIKfyve inhibitors and stimulated with zymosan as in (A) before fixation and staining for CatS (red in merge). Yellow arrowheads, CatS-positive phagosomes. Scale bar, 10 μm.

(E) Quantification of (D) for cells stimulated with zymosan for 0.5 or 1 hr (>133 phagosomes per condition per donor; mean ± SEM of three donors; individual donors shown; normalized to the total number of phagosomes per cell).

*P < 0.05, **P < 0.01, ***P < 0.001. See also Figures S2 and S3.

and S2F) at the phagosomes, indicating that trafficking of CatS to phagosomes is reduced by PIKfyve inhibitors. To determine whether the reduced CatS activity was solely attributable to its reduced recruitment to phagosomes upon PIKfyve inhibition, we performed experiments with BMV109 in lysates of dendritic cells (Figure S3A). For some conditions, apilimod and YM201636 still reduced the signal of BMV109 for CatS, whereas the signals for cathepsins B and X were unaltered (Figures S3B and S3C). We conclude that the reduced CatS activity upon PIKfyve inhibition is not solely due to altered trafficking, because CatS activity is also reduced in cell lysates.

CatS is expressed at high levels by dendritic cells and has a strong immunological relevance, because it controls the generation of CLIP (Honey and Rudensky, 2003; Riese et al., 1996; Villadangos and Ploegh, 2000). Within endolysosomes, CLIP is derived from the invariant chain Ii via the intermediate fragments Iip23 and Iip10 (Amigorena et al., 1995; Neefjes and Ploegh, 1992; Villadangos et al., 2000). The final processing of Iip10 into CLIP is mediated by CatS. The inhibition or loss of CatS in mice (Nakagawa et al., 1999; Shi et al., 1999) causes accumulation of Iip10-bound MHC class II in endo/lysosomal compartments, impeding MHC class II trafficking to the cell surface (Brachet et al., 1997; Riese and Chapman, 2000). As inhibition of PIKfyve results in reduced activity of CatS, we hypothesized that apilimod and YM201636 would cause a defect of Ii processing and MHC class II trafficking. To address this hypothesis, we first assessed the effects of apilimod or YM201636 treatment on plasma membrane localization of MHC class II. Flow cytometry experiments with an antibody recognizing the extracellular domain of MHC class II revealed that apilimod or YM201636 treatment caused a small (~10%–20%) but consistent reduction of the presence of MHC class II at the plasma membrane (Figures 4A and 4B). In contrast, total cellular levels of MHC class II, measured by immunolabeling in the presence of a detergent, were unaltered or even (inconsistently) increased (Figure 4C). Similar observations were made with dendritic cells derived from mouse bone marrow (Figures S4A–S4C). We also performed flow cytometry experiments with an antibody recognizing Ii or CLIP-bound to αβMHC class II (clone CerCLIP.1; Denzin et al., 1994), revealing that the presence of this inactive form of MHC class II was also reduced at the plasma membrane, whereas the total cellular levels were increased (Figures S4D–S4F). The defect in processing of CLIP upon PIKfyve inhibition was also observed by western blot with mouse bone-marrow-derived dendritic cells using an antibody recognizing the Iip10 fragment (Figures S4G and S4H). Here, we used the CatS inhibitor LHVS (morpholinurea-leucine-homophenylalanin-vinylsulfone-phenyl) as a positive control (Palmer et al., 1995; Riese et al., 1998). A direct inhibition of CatS with LHVS also had a similar effect on MHC class II trafficking as PIKfyve inhibition with apilimod or YM201636 (Figures S4I and S4J). Microscopy imaging of phagocytic cells overexpressing fluorescently tagged MHC class II (Zwart et al., 2005) showed that MHC class II is recruited to phagosomes after zymosan uptake (Video S3). Immunofluorescence microscopy showed that treatment with PIKfyve inhibitors showed increased accumulation of endogenous MHC class II on the phagosomes (Figures 4D and 4E), suggesting a trafficking defect. Together, these results show that PIKfyve supports CatS activity and thereby regulates the proteolytic activation of MHC class II.

The Inactivation of Cathepsin S upon PIKfyve Inhibition Is due to Oxidative Modifications

In dendritic cells, NOX2 produces large amounts of ROS within the lumen of endosomes and phagosomes, and this ROS production is sustained for hours after uptake (Dingjan et al., 2016, 2017a, 2017b; Jancic et al., 2007; Joffre et al., 2012; Kotsias et al., 2013; Mantegazza et al., 2008; Nunes et al., 2013; Savina et al., 2006; Vulcano et al., 2004). ROS alter the processing of the ingested antigen for MHC classes I and II presentation (Hari et al., 2015; Mantegazza et al., 2008; Rybicka et al., 2012), with one of the mechanisms being the oxidative modification of a cysteine located within the catalytic site of CatS (Allan et al., 2014; Hari et al., 2015; Jancic et al., 2007; Kanai et al., 2001; Rybicka et al., 2012). In line with this, treatment of cells with the membrane-permeable organometallic compound phenylarsine oxide, which modifies cysteines, resulted in an inhibition of CatS, but not or less of cathepsins B and X (Figures 5A and 5B), indicating that the activity of CatS is particularly sensitive to cysteine modifications. We recently showed that NOX2 is already present at nascent phagosomes, because the catalytic subunit gp91^{phox} of NOX2 is co-invaginated from the plasma

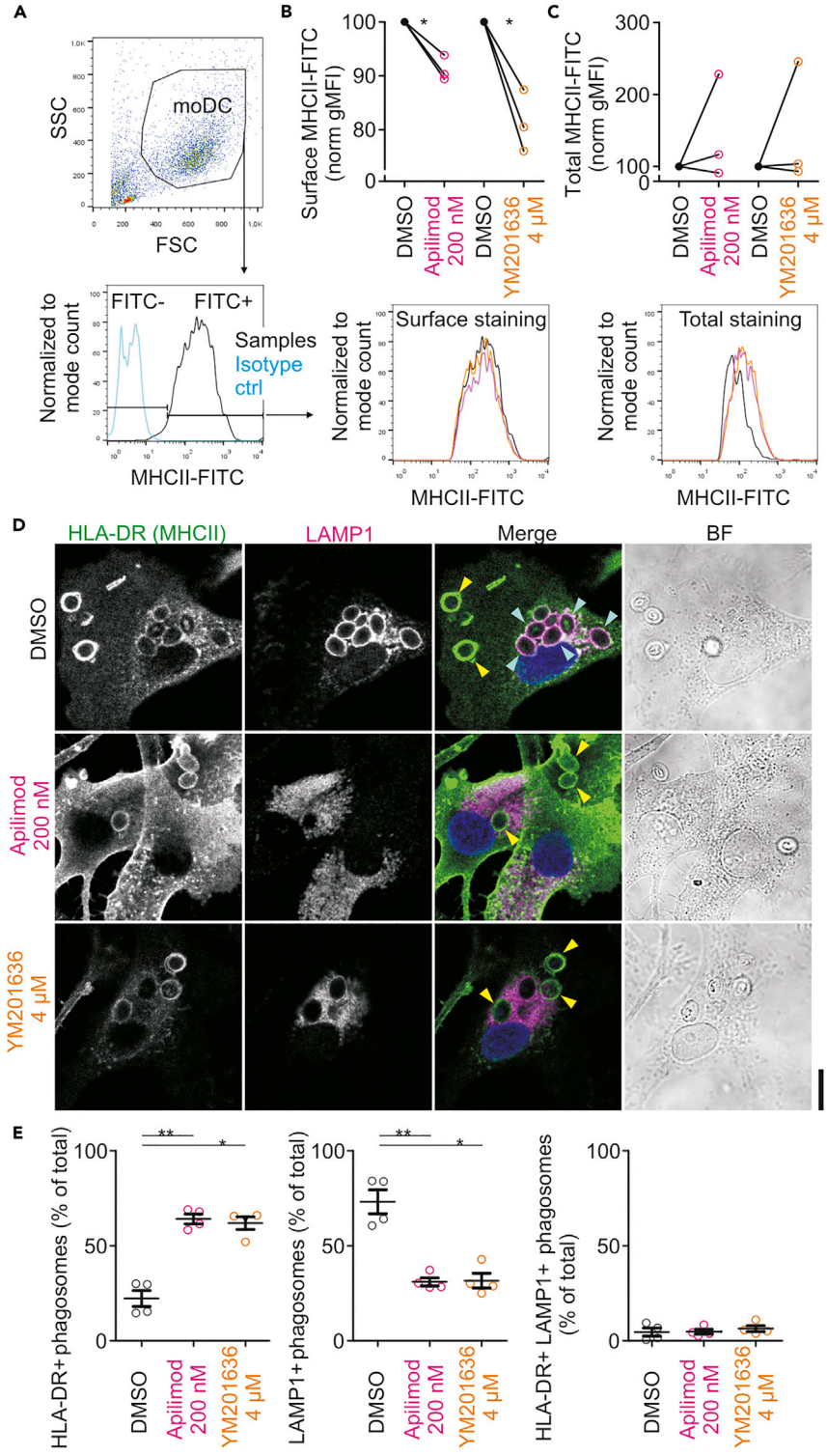

Figure 4. Pharmacological Inhibition of PIKfyve Impairs Proteolytic Activation and Trafficking of MHC Class II

(A) Gating strategy for flow cytometry of human-monocyte-derived dendritic cells immunolabeled for MHC class II (MHCII-FITC; HLA-DR, DQ). Light blue in histogram, isotype control; SSC, side scatter; FSC, forward scatter; FITC, fluorescein isothiocyanate.

Figure 4. *Continued*

(B) Representative histograms and quantification of surface MHC class II with flow cytometry experiments of dendritic cells treated for 3 hr with apilimod (200 nM) or YM201636 (4 μM) (geometric mean fluorescence intensities [gMFI]; individual donors shown; normalized to DMSO control).

(C) Same as (B), but now for total MHC class II with detergent permeabilization.

(D) Confocal images of representative dendritic cells treated with apilimod (200 nM) or YM201636 (4 μM) for 3 hr and pulsed with zymosan 1 hr before fixation. DMSO, vehicle control. Cells were immunolabeled for HLA-DR (green in merge) and LAMP1 (magenta in merge). Blue, DAPI staining. BF, brightfield. Scale bar, 10 μm. Yellow arrowheads, HLA-DR-positive phagosomes; cyan arrowheads, LAMP1-positive phagosomes.

(E) Quantification of percentages of HLA-DR-positive and LAMP1-positive phagosomes from (D) normalized to the total number of phagosomes per cell (~280 phagosomes per condition per donor; mean ± SEM of four donors).

*P < 0.05, **P < 0.01, ***P < 0.001. See also Figures S4–S6.

membrane together with the antigen during phagocytosis (Dingjan et al., 2017a). Moreover, NOX2 requires the presence of $PI(3,4)P_2$ and/or PI(3)P for its activity and is active on early phagosomes (Anderson et al., 2010; Ellson et al., 2001b; Groemping and Rittinger, 2005; Kanai et al., 2001). We also showed that even though NOX2 resides in lysosomal compartments in naive dendritic cells, it is gradually removed from phagosomes during their conversion into LAMP1-positive phagolysosomes (Dingjan et al., 2017a, 2017b). As our data show that blockage of PIKfyve led to an accumulation of PI(3)P on phagosomes (Figures 2C and 2D) and delayed the conversion of early into late endo/phagosomes, we hypothesized that the reduced CatS activity was caused by an increased ROS production resulting from a prolonged presence and increased activity of NOX2. The presence of phagosomal NOX2 upon PIKfyve inhibition by apilimod and YM201636 was assessed using immunofluorescence staining for its main catalytic subunit $gp91^{phox}$ (Dingjan et al., 2017a, 2017b). Treatment with apilimod and YM201636 resulted in a prolonged presence of $gp91^{phox}$ at zymosan-containing phagosomes compared with the DMSO control (Figures 5C and 5D). We also measured ROS production in cells pulsed for 1 hr with zymosan using two different assays. First, apilimod treatment resulted in an increased extracellular presence of H_2O_2 as measured with the Amplex Red assay (Dingjan et al., 2016) (Figure 5E). Second, intra-phagosomal ROS production was measured with zymosan particles conjugated to the ROS-sensitive probe OxyBURST (Dingjan et al., 2017a), and this also showed an increased ROS production upon PIKfyve inhibition with apilimod or YM201636 (Figures 5F and 5G). Our data suggest that CatS is more sensitive to oxidative modifications than other cathepsins, and the increased ROS production upon PIKfyve inhibition can thereby explain the reduced activity of CatS (but not B and X) in cell lysates (Figure S3). Together, we conclude that PIKfyve inhibition results in an increased production of ROS within endo/phagosomes and that this leads to a reduced activity of CatS, which is more prone to oxidative modifications than cathepsins B and X.

PIKfyve Inhibition Impairs MHC Class II Presentation

In the final set of experiments, we tested whether inhibition of PIKfyve would lead to impaired MHC class II antigen presentation. We first performed a classical T cell activation assay with T cells isolated from transgenic OT-II mice (Barnden et al., 1998). $CD4^+$ T cells from these mice carry a T cell receptor specifically recognizing ovalbumin residues 323–339 ($OVA_{323-339}$) presented on $H\text{-}2IA^b$ MHC class II. Apilimod treatment resulted in an ~25% reduction of production of interferon (IFN) γ by the OT-II T cells over time, whereas YM201636 even completely blocked IFNγ release (Figures S5A and S5B). However, the long incubation times with apilimod or YM201636 required for T cell activation, reduced the viabilities of both the dendritic cells and OT-II T cells by 20%–40% (Figures S5C and S5D). Moreover, as expected, surface presentation of MHC class II in those experiments was reduced by ~10-30% upon PIKfyve inhibition (Figures S5E and S5F). Because of these effects, the impaired activation of T cells upon PIKfyve inhibition cannot be solely attributed to lower antigen presentation. Indeed, control experiments showed that both apilimod and especially YM201636 blocked T cell activation independent of antigen presentation, as these compounds resulted in reduced production of IFNγ and lower surface expression of the activation markers CD25 and CD69 (Figure S6). Thus, although we observed a reduction of T cell activation by inhibition of PIKfyve, this is probably mainly caused by direct effects of apilimod and YM201636 on the T cells and the T cell activation assay does not allow to discern direct effects on MHC class II presentation.

To overcome this problem, we developed a new method allowing for direct visualization of MHC class II presentation. This is based on a recently developed assay for visualization of MHC class I presentation (Pawlak et al., 2015, 2016), and employs synthetic peptides as antigen carrying a non-natural amino acid

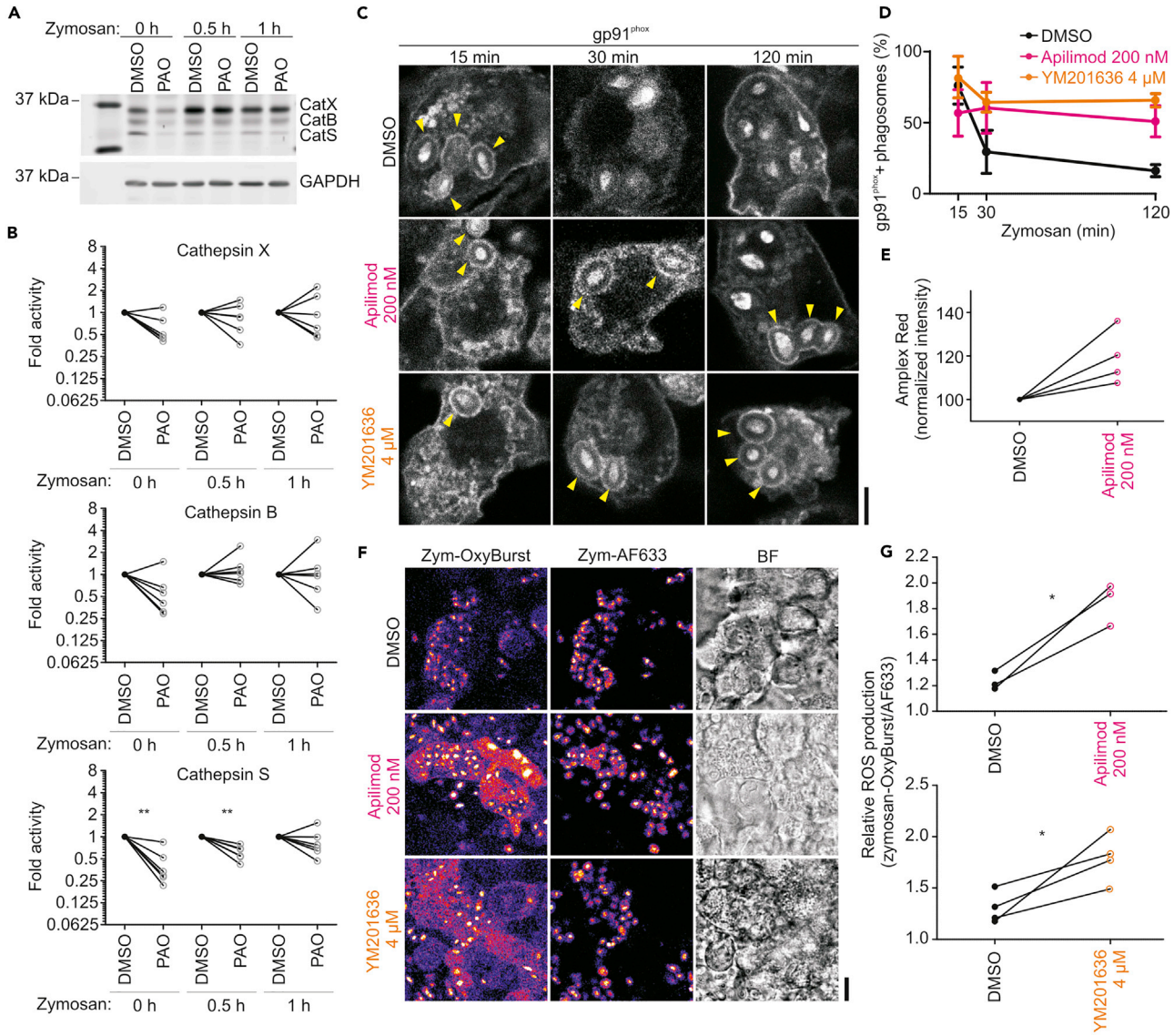

Figure 5. Pharmacological Inhibition of PIKfyve Promotes NOX2-Mediated ROS Production

(A) SDS-PAGE with in-gel fluorescence for the cathepsin-activity-based probe BMV109-Cy5 for dendritic cells pulsed with zymosan for 0.5 or 1 hr and untreated (0 hr). PAO, cysteine-modifying agent phenylarsine oxide; DMSO, vehicle control; GAPDH, loading control by western blot.

(B) Quantification of (A) (individual donors shown; normalized to DMSO controls).

(C) Confocal images of representative dendritic cells pulsed with zymosan for 15, 30, or 120 min in the presence of apilimod (200 nM) or YM201636 (4 µM) for 3 hr and immunostained for $gp91^{phox}$. Yellow arrowheads, $gp91^{phox}$-positive phagosomes. Scale bar, 5 µm.

(D) Quantification of (C); $Gp91^{phox}$-positive phagosomes were counted and normalized to the total number of phagosomes per cell (mean ± SEM for three donors, ~300 phagosomes per condition).

(E) Extracellular H_2O_2 measurements with Amplex Red assay for dendritic cells treated for 3 hr with apilimod and 1 hr with zymosan.

(F and G) Phagosomal ROS production determined with zymosan labeled to both OxyBURST and Alexa Fluor 633 (AF633) and confocal live imaging. Cells were treated for 3 hr with apilimod (F) or YM201636 (G) and incubated for 1 hr with zymosan-OxyBURST/AF633. Signals from OxyBURST signal were normalized to that of AF633 (~3,000 phagosomes per condition; individual donors shown). *P < 0.05, **P < 0.01, ***P < 0.001.

amendable to bio-orthogonal ligation with fluorescent dyes. Based on the crystal structure of a complex of human HLA-DR1 MHC class II with influenza A virus hemagglutinin (HA) (strain A/Aichi/2/1968 H3N2) peptide (322–334 amino acid positions; PKYVKQNTLKLAT; $HA_{322-334}$) (Stern et al., 1994; Zavala-Ruiz et al., 2004), we synthesized a peptide consisting of the MHC class II epitope of influenza extended both N and C terminally with four natural amino acids (YGACPKYVKQNTLKLATGMRN; $HA_{318-338}$) (Figure S7, related to Table S1). This extended peptide needs to be processed and loaded by HLA-DM in MIIC to

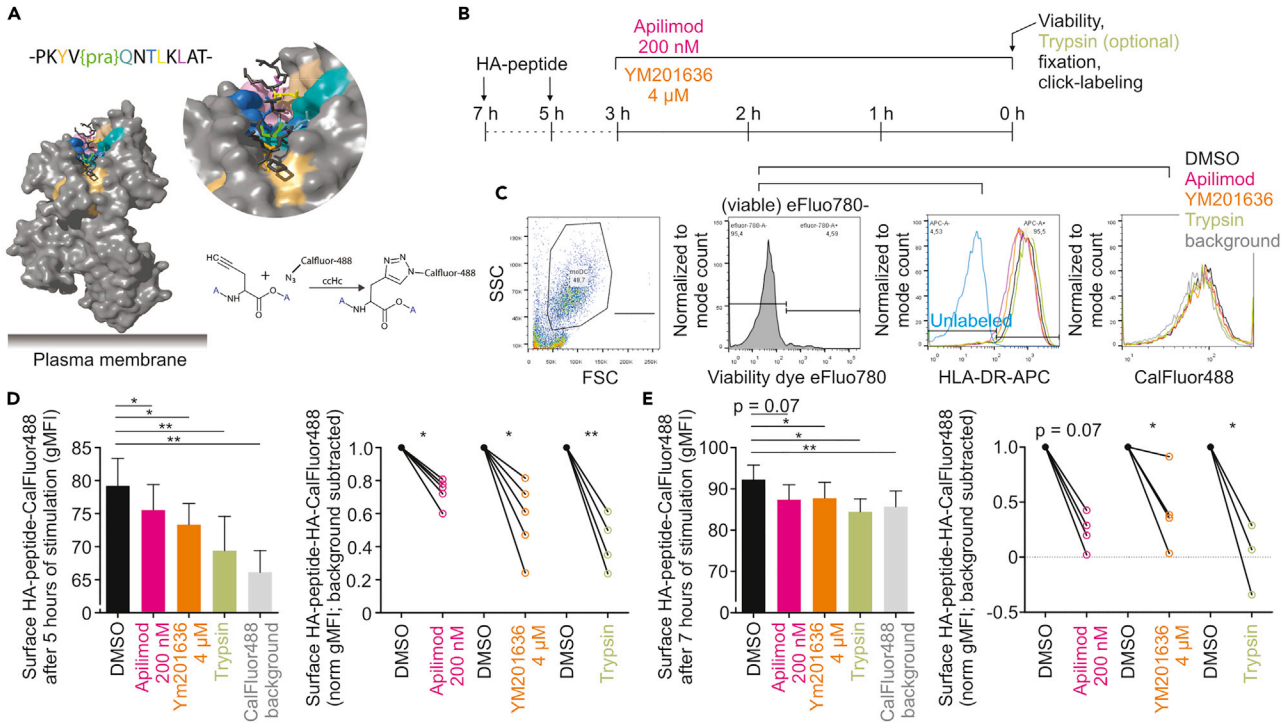

Figure 6. PIKfyve Inhibition Impairs MHC Class II Presentation

(A) Crystal structure of human HLA-DR1 (DRA, DRB1*0101; PDB: 1DLH) in complex with a virus HA (strain A/Aichi/2/1968 H3N2) peptide residues 322–334. The position of a clickable non-naturalized amino acid L-C-propargylglycine {pra} for bio-orthogonal labeling with CalFluor-488 is indicated (bright green); pockets for peptide binding at the HLA-DR1 cleft are highlighted in different colors. A scheme of the bio-orthogonal reaction is also shown.

(B) Time line of stimulation with HA peptide residues 318–338 for MHC class II presentation by human dendritic cells.

(C) Flow cytometry gating strategy for quantification of HLA-DR1 presented HA by labeling with CalFluor-488 as depicted in (A and B). Cell viability was assessed with fixable viability dye eFluo780. Surface levels of HLA-DR1 were assessed with HLA-DR-APC.

(D) Quantification of HA-CalFluor-488 signals from (C) after 5 hr of stimulation with HA-peptide (bar graphs). Gray, non-specific background from CalFluor labeling of dendritic cells that were not incubated with HA-peptide; green, trypsin-positive control for HA removal from the cell surface; line graphs, individual donors with background subtracted and normalized to DMSO control.

(E) The same as (D), but now for 7 hr of stimulation with HA peptide.

*P < 0.05, **P < 0.01, ***P < 0.001. See also Figures S7 and S8 and Table S1.

be presented on MHC class II. The central lysine (K326) was converted into a propargylglycine. Modeling indicated that the alkyne moiety of propargylglycine is solvent accessible when this peptide is bound to MHC class II (Figure 6A). This alkyne moiety can be conjugated to CalFluor-488, which increases the fluorescence signal by two orders of magnitude, resulting in a low signal-to-noise ratio (Shieh et al., 2015). Moreover, the alkyne moiety is only three carbon atoms in size and does not (or less) perturb the molecular mechanisms of antigen processing and presentation, in contrast to large fluorophores, and survives the harsh environment in lysosomes (Bakkum et al., 2018). By incubating human dendritic cells with bio-orthogonal functionalized peptide $HA_{318-338}$, we could show increased MHC class II presentation over time for at least up to 5-hr incubation (Figures 6B–6D and S8). Moreover, no increase in CalFluor-488 signal was observed with negative control experiments with a wild-type $HA_{318-338}$ peptide (without propargylglycine) or the $HA_{322-334}$ epitope, which cannot be processed for HLA-DM loading onto MHC class II, or by proteolytically cleaving surface-exposed MHC class II with trypsin. Compared with the 5-hr time point, longer incubation (18 hr) led to reduction of the CalFluor-488 signal, suggesting that the peptide was internalized and/or degraded by the cells (Figure S8). When apilimod or YM201636 was present during the last 3 hr of 5- or 7-hr incubation with the bio-orthogonally functionalized peptide $HA_{318-338}$, the signals from CalFluor-488 were consistently reduced by 20%–80% (depending on the donor) (Figures 6C–6E), demonstrating that these drugs directly blocked presentation of the HA antigen. Thus using bio-orthogonal functionalized antigenic peptide, we could demonstrate that blockage of PIKfyve leads to impaired MHC class II antigen presentation.

DISCUSSION

In this study, we studied the role of PIKfyve in MHC class II antigen presentation by dendritic cells. Our data confirm the key role of PIKfyve in phagosome maturation (Compton et al., 2016; Dayam et al., 2017; Dove et al., 2009; Gayle et al., 2017a; Gomez et al., 2018; Hazeki et al., 2012; Ikonomov et al., 2009; Kerr et al., 2010; Kim et al., 2014b; Krishna et al., 2016; Sbrissa et al., 2007, 2012) and treatment of dendritic cells with apilimod and YM201636 blocked recruitment of LAMP1, M6PR, and CatS to phagosomes. A still open question is via which mechanisms the reduced levels of cellular $PI(3,5)P_2$ cause these trafficking defects. Endosomal maturation via the conversion of Rab5- to Rab7-positive membranes by the endosomal tethering complexes CORVET (class C core vacuole/endosome tethering) and HOPS (homotypic fusion and protein sorting) is well understood (Balderhaar and Ungermann, 2013). The role of $PI(3,5)P_2$ and downstream effectors of $PI(3,5)P_2$ in endosomal maturation is uncertain, and $PI(3,5)P_2$ might govern trafficking events via several possible mechanisms. The best characterized downstream effector of $PI(3,5)P_2$ is the cation channel TRPML1; its activity directly depends on $PI(3,5)P_2$. However, it is also not known if and how TRPML1 affects endo/phagosomal maturation. As TRPML1 triggers the efflux of Ca^{2+} from lysosomes to the cytosol, one possibility is that it might be able to activate ALG-2, a dynein-interacting protein sensitive to Ca^{2+}. Dyneins promote retrograde vesicular migration along the tubular tracks, and this might somehow facilitate endosome-lysosome fusion (Li et al., 2016). Alternatively or additionally, the increased Ca^{2+} efflux might directly promote intracellular fusion events via Ca^{2+}-sensing proteins (Hay, 2007). Another downstream effector of $PI(3,5)P_2$ is the V-ATPase, as yeast strains with mutations in the PIKfyve ortholog Fab1p showed impaired vacuolar acidification (Li et al., 2014), and this might explain the reduced acidification upon pharmacological inhibition or siRNA knockdown of PIKfyve.

Our results showed that the blockage of phagosome maturation by PIKfyve inhibition resulted in reduced activity of CatS and B, but not of cathepsin X. Our data suggest that the reduced activity of CatS upon apilimod or YM201636 treatment might be attributed to both a reduced trafficking to phagosomes and an increased ROS production by NOX2. Our microscopy data show that CatS trafficking to LAMP1-positive phagosome relies on PIKfyve activity. Moreover, we showed that NOX2-produced ROS affect cysteine cathepsins, including CatS, because the ROS can modify cysteines within their catalytic cores (Allan et al., 2014; Hari et al., 2015; Jancic et al., 2007; Rybicka et al., 2012). The increased ROS production caused by a prolonged presence of NOX2 at phagosomes upon apilimod or YM201636 treatment might even be amplified by higher phagosomal levels of PI(3)P, which might enhance NOX2 activity through NOX2 subunit $p40^{phox}$ binding to PI(3)P by its PX domain (Anderson et al., 2010; Ellson et al., 2001b; Groemping and Rittinger, 2005; Kanai et al., 2001). An open question is why addition of zymosan reduced the inactivation of cathepsin B and S. As we also observe this effect in our lysate controls, perhaps the zymosan particles sequester ROS species and thereby prevent the oxidative modification of CatS. This suggests that the NOX2-mediated reduction of CatS activity will mainly have physiological relevance in the absence of phagocytic cargo, and thereby might be involved in the maintenance of self-tolerance (Steinman and Nussenzweig, 2002), for instance, for the induction of Th2 responses by immature dendritic cells (Na et al., 2016). In any case, our data show that PIKfyve-mediated phagosomal maturation affects the activity of cysteine cathepsins via NOX-produced ROS, and this can modulate the epitope repertoire for MHC presentation (Balce et al., 2011; Rybicka et al., 2010, 2012). Because NOX2 mediates the disulfide reduction of protein antigens (Ewanchuk and Yates, 2018), the effects of NOX2-produced ROS on antigen processing will be even more pronounced. Only linear peptide/protein stretches are accessible to proteases for cleavage, hence all inter- and intra-disulfide bonds have to be reduced before antigen processing (Bogunovic et al., 2010), as has been also demonstrated for MHC class II with model antigens (Jensen, 1991). γ-Interferon-inducible lysosomal thiol reductase activity can be inhibited by ROS, and this may cause different antigen processing patterns leading to altered repertoires of peptides for presentation, because some of the proteins cannot be unfolded and are therefore not accessible to proteinases for degradation (Ewanchuk and Yates, 2018).

In addition to the proteolytic processing of ingested antigens, CatS mediates the activation of MHC class II in MIIC via the processing of Ii to CLIP and is thereby required for antigen presentation (Nakagawa et al., 1999; Riese and Chapman, 2000; Shi et al., 1999). Our data show that inhibition of PIKfyve by apilimod or YM201636 results in an accumulation of Iip10, the precursor of CLIP, and in reduced trafficking of MHC class II to the cell surface. This is in line with the finding that the inhibitor of PIKfyve AS2795440 caused a marked reduction of surface MHC class II expression on $CD45R^+$ B cells in anti-IgM-stimulated whole blood from rats (Terajima et al., 2016). These findings can be explained by the decreased activity of CatS, as incomplete

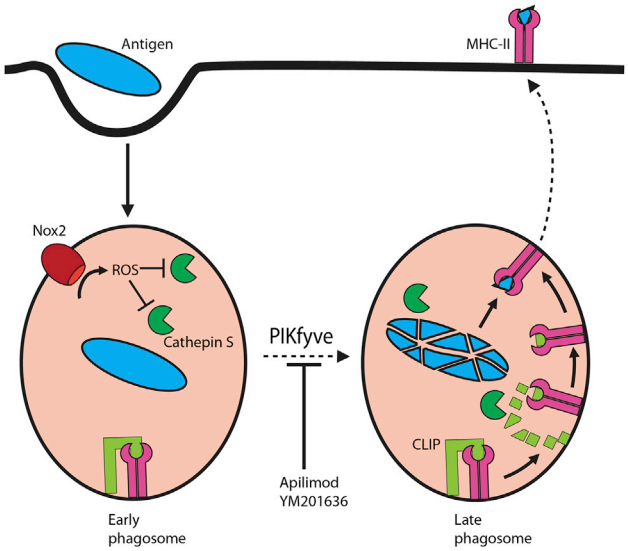

Figure 7. Delayed Phagosomal Maturation Results in a Reduced MHC Class II Antigen Presentation

Model figure showing antigen uptake by a dendritic cell and subsequent processing within phagosomes by ROS and cathepsins. Upon phagosomal maturation, MHC class II bound to Ii is trafficked to the phagosome where cathepsin S is involved in the processing of Ii to CLIP, which can then be exchanged by an antigen to be presented by MHC class II on the cell surface. Inhibiting PIKfyve delays phagosomal maturation, and due to prolonged ROS formation, cathepsin S becomes oxidized and deactivated, thereby blocking CLIP-to-antigen exchange and eventually resulting in impaired antigen presentation.

invariant chain degradation is known to result in disturbance of MHC class II presentation and blockage of MHC class II transfer from endocytic compartments to the cell surface (Brachet et al., 1997; Riese and Chapman, 2000), as confirmed by our experiments with the CatS inhibitor LHVS. The proteolytic truncation of Ii to MHC-class-II-bound CLIP peptide is a prerequisite for antigen loading and thereby for MHC class II antigen presentation (Roche and Furuta, 2015), and surface trafficking of MHC class II is important for successful antigen presentation (Rocha and Neefjes, 2008). This might explain the reduced presentation of influenza virus $HA_{322–334}$ on HLA-DR1 by human dendritic cells upon YM201636 or apilimod treatment. Unsurprisingly, we also observed reduced activation of $CD4^+$ T cells upon PIKfyve inhibition, although this is probably caused by the combined effects of (1) reduced uptake of antigen, (2) blocked production of IL-12/IL-23 and type I IFN (Cai et al., 2013, 2014), (3) reduced MHC class II presentation, (4) reduced cell viability of both the dendritic cells and T cells, and (5) other direct effects of apilimod and YM201636 on T cells.

To overcome this, we developed a new universal assay allowing for the direct visualization of MHC class II antigen presentation. This assay is an adaptation of a recent assay to measure antigen presentation on MHC class I (Pawlak et al., 2015, 2016) and is based on synthetic peptides containing an MHC class-II-compatible epitope (in this case from HA residues 318–338 containing epitope residues 322–334). One residue on the epitope, which remains solvent exposed when bound to MHC class II, is converted to a non-natural propargylglycine, which contains an alkyne moiety of only three atoms in size. In contrast to large fluorescent labels, peptides carrying propargylglycine can still be proteolytically processed and loaded onto MHC class II. After fixation of the cells, the peptide bound to MHC class II at the surface of the dendritic cells can be labeled with CalFluor dyes that increase in fluorescence signal by orders of magnitude (Shieh et al., 2015). As previously shown for MHC class I (Pawlak et al., 2015, 2016), this signal increase allows for the detection of the limited amounts of MHC class-II-presented epitopes by flow cytometry. In contrast to assays that assess T cell priming and rely on co-stimulatory factors, such as the OT-II assay, the assay developed in this study provides a direct and quantitative readout of MHC class II presentation and is easily adaptable for different antigens and MHC haplotypes.

In conclusion, we showed that the phagosomal maturation driven by phosphoinositide kinase PIKfyve is essential for MHC class II antigen presentation (Figure 7). Disruption of this process by the PIKfyve inhibitors apilimod and YM201636 delays the maturation process of the phagosome. Delayed phagosomal

maturation, in turn, results in elevated levels of ROS thereby deactivating CatS, which plays a key role in the proteolytic cleavage of Ii to CLIP and is essential for MHC class II antigen presentation. PIKfyve inhibition results in an incomplete processing of CLIP, and Ii-bound MHC class II is retained in phagosomes. Apilimod is proposed as a promising treatment for multiple variations of B cell non-Hodgkin lymphoma (NHL) due to its cytotoxic effect on B-NHL cancer cells lines (Gayle et al., 2017b) and was used in clinical trials for blocking IL-12/IL-23-mediated Th1/17 pro-inflammatory response in Crohn disease, psoriasis, and rheumatoid arthritis (Burakoff et al., 2006; Krausz et al., 2012; Sands et al., 2010; Wada et al., 2007, 2012). As concluded from NHL cancer cell line experiments, these cells have maximal sensitivity to apilimod, due to non-understood modulatory effects of $PI(3,5)P_2$ on the transcription factor TFEB and apilimod leading to elevated expression of genes coding for lysosomal proteins, resulting in lysosomal swelling and disruption of lysosomal homeostasis and maturation, proliferation block, and cell death. In addition, PIKfyve might be a potential target for targeting solid tumors, as it plays a role in metastasis and promotes cancer cell migration and invasion together with the phosphoinositide phosphatase myotubularin-related protein 3 (MTMR3), which converses $PI(3,5)P_2$ to PI(5)P (Oppelt et al., 2014). Depletion of PIKfyve and MTMR3, as well as inhibition of PIKfyve alone by YM201636, resulted in decreased *in vitro* migration of cancer cell lines of lung, rhabdomyosarcoma, and osteosarcoma origins (Oppelt et al., 2014), indicating that PIKfyve could be a novel therapeutic target in cancer migration. However, our results show that inhibition of PIKfyve impairs antigen presentation by dendritic cells and reduces activation of T cells. These effects on immune activation must be taken into account in clinical trials targeting PIKfyve.

Limitations of the Study

In this study, we addressed the role of phagosomal and endosomal maturation of MHC class II presentation with a focus on the phosphoinositide kinase PIKfyve. Most of our results are obtained using the small molecule inhibitors that are shown to be specific for PIKfyve: apilimod (Cai et al., 2013) and YM201636 (Jefferies et al., 2008). We confirmed that PIKfyve inhibition with these compounds was similar to PIKfyve siRNA knock down in primary human monocyte-derived dendritic cells, and both resulted in formation of enlarged endosomes, delayed phagosomal acidification, and delayed LAMP1 recruitment. However, the efficiency of our siRNA knockdown was incomplete, leading to less pronounced functional effects compared with the inhibitors. Our work could benefit from stable knockdown/out of PIKfyve to demonstrate that all experiments with drug inhibitors are comparable to knockout. However, the primary human monocyte-derived dendritic cells used in our study are terminally differentiated and not amenable to CRISPR/Cas knockout.

A potential caveat of our study is that we only managed to immunolabel endogenous CatS, but not the other two cathepsins X and B. Therefore we cannot draw clear conclusions on the effects of PIKfyve inhibition on the trafficking of those cathepsin species.

We admit that MHC class II labeling with CalFluor-488 method has still some limitations, mainly a low signal-to-noise ratio, which is likely caused by a low number of MHC-class-II-presented epitopes. Additional optimizations of this method will be required in future.

In our live cell microscopy experiments we followed the trafficking of MHC class II to phagosomes, revealing that a large portion of it is recruited from the cell surface during formation of the phagosome. However, we only followed the fate of MHC class II during PIKfyve inhibition for a short time and never studied longer time points after zymosan uptake. It would be interesting to determine whether MHC class II also reaches phagosomes from an intracellular pool, as we recently showed for NOX2 (Dingjan et al., 2017a).

Our study raises the key open question as to which effectors of $PI(3,5)P_2$ mediate phagosomal maturation, as explained in the Discussion section. It would be interesting to identify those in the future.

METHODS

All methods can be found in the accompanying Transparent Methods supplemental file.

SUPPLEMENTAL INFORMATION

Supplemental Information includes Transparent Methods, eight figures, one table, and three videos and can be found with this article online at https://doi.org/10.1016/j.isci.2018.12.015.

ACKNOWLEDGMENTS

We thank Michael Sixt for LifeAct-RFP construct, Assia Shisheva for pEGFP-HA-PIKfyve and pEGFP-HA-PIKfyveK1831E, Jacques Neefjes for the MHC-II-YFP construct, and Matthew Bogyo for the LHVS. The authors express their gratitude to Yusuf Dölen for providing OT-II cells and PLGA-OVA, and Olga Ilina for OT-I cells. This work was supported by a Starting Grant from the European Research Council (ERC) under the European Union's Seventh Framework Program (Grant Agreement 336479). G.v.d.B. is funded by a Hypatia fellowship from the Radboud University Medical Center, a Career Development Award from the Human Frontier Science Program, the NWO Gravitation Program 2013 (ICI-024.002.009), and a Vidi grant from the Netherlands Organisation for Scientific Research (NWO-ALW VIDI 864.14.001). F.B. is funded by an EMBO Short-Term fellowship (7280) and a Veni grant from the Netherlands Organization for Scientific Research (016.Veni.192.026). Work from C.R.B.'s laboratory at Stanford University was supported by the NIH grant R37 GM058867.

AUTHOR CONTRIBUTIONS

Conceptualization: M.V.B., F.B., and G.v.d.B.; Methodology: F.B., S.M., E.M.M., M.V.B., and G.v.d.B.; Investigation: M.V.B., M.A.C.v.A, F.B., S.M., A.M., I.D., and M.t.B; Writing – Original Draft: M.V.B and G.v.d.B; Writing – Review & Editing: F.B., M.V. and M.t.B.; Visualization: M.V.B., F.B, G.v.d.B.; CalFluor labeling: C.R.B. and S.G.L.K; peptide synthesis: A.S. and U.D.; activity-based probes: M.V.; Resources: G.v.d.B., M.V., U.D., and C.R.B; Supervision: G.v.d.B.; Funding Acquisition: G.v.d.B.

DECLARATION OF INTERESTS

The authors declare no competing interests.

Received: June 25, 2018
Revised: November 28, 2018
Accepted: December 14, 2018
Published: January 25, 2019

REFERENCES

Allan, E.R., Tailor, P., Balce, D.R., Pirzadeh, P., McKenna, N.T., Renaux, B., Warren, A.L., Jirik, F.R., and Yates, R.M. (2014). NADPH oxidase modifies patterns of MHC class II-restricted epitopic repertoires through redox control of antigen processing. J. Immunol. *192*, 4989–5001.

Amigorena, S., Drake, J.R., Webster, P., and Mellman, I. (1994). Transient accumulation of new class II MHC molecules in a novel endocytic compartment in B lymphocytes. Nature *369*, 113–120.

Amigorena, S., Webster, P., Drake, J., Newcomb, J., Cresswell, P., and Mellman, I. (1995). Invariant chain cleavage and peptide loading in major histocompatibility complex class II vesicles. J. Exp. Med. *181*, 1729–1741.

Anderson, K.E., Chessa, T.A., Davidson, K., Henderson, R.B., Walker, S., Tolmachova, T., Grys, K., Rausch, O., Seabra, M.C., Tybulewicz, V.L., et al. (2010). PtdIns3P and Rac direct the assembly of the NADPH oxidase on a novel, pre-phagosomal compartment during FcR-mediated phagocytosis in primary mouse neutrophils. Blood *116*, 4978–4989.

Bakkum, T., van Leeuwen, T., Sarris, A.J.C., van Elsland, D.M., Poulcharidis, D., Overkleeft, H.S., and van Kasteren, S.I. (2018). Quantification of bioorthogonal stability in immune phagocytes using flow cytometry reveals rapid degradation of strained alkynes. ACS Chem. Biol. *13*, 1173–1179.

Balce, D.R., Li, B., Allan, E.R., Rybicka, J.M., Krohn, R.M., and Yates, R.M. (2011). Alternative activation of macrophages by IL-4 enhances the proteolytic capacity of their phagosomes through synergistic mechanisms. Blood *118*, 4199–4208.

Balderhaar, H.J., and Ungermann, C. (2013). CORVET and HOPS tethering complexes - coordinators of endosome and lysosome fusion. J. Cell Sci. *126*, 1307–1316.

Banchereau, J., and Steinman, R.M. (1998). Dendritic cells and the control of immunity. Nature *392*, 245–252.

Baranov, M.V., Revelo, N.H., Dingjan, I., Maraspini, R., Ter Beest, M., Honigmann, A., and van den Bogaart, G. (2016). SWAP70 organizes the actin cytoskeleton and is essential for phagocytosis. Cell Rep. *17*, 1518–1531.

Baranov, M.V., Revelo, N.H., Verboogen, D.R.J., Ter Beest, M., and van den Bogaart, G. (2017). SWAP70 is a universal GEF-like adaptor for tethering actin to phagosomes. Small GTPases. in press. https://doi.org/10.1080/21541248.2017.1328302.

Barnden, M.J., Allison, J., Heath, W.R., and Carbone, F.R. (1998). Defective TCR expression in transgenic mice constructed using cDNA-based alpha- and beta-chain genes under the control of heterologous regulatory elements. Immunol. Cell Biol. *76*, 34–40.

Bissig, C., Hurbain, I., Raposo, G., and van Niel, G. (2017). PIKfyve activity regulates reformation of terminal storage lysosomes from endolysosomes. Traffic *18*, 747–757.

Blum, J.S., Wearsch, P.A., and Cresswell, P. (2013). Pathways of antigen processing. Annu. Rev. Immunol. *31*, 443–473.

Bogunovic, B., Srinivasan, P., Ueda, Y., Tomita, Y., and Maric, M. (2010). Comparative quantitative mass spectrometry analysis of MHC class II-associated peptides reveals a role of GILT in formation of self-peptide repertoire. PLoS One *5*, e10599.

Brachet, V., Raposo, G., Amigorena, S., and Mellman, I. (1997). Ii chain controls the transport of major histocompatibility complex class II molecules to and from lysosomes. J. Cell Biol. *137*, 51–65.

Burakoff, R., Barish, C.F., Riff, D., Pruitt, R., Chey, W.Y., Farraye, F.A., Shafran, I., Katz, S., Krone, C.L., Vander Vliet, M., et al. (2006). A phase 1/2A trial of STA 5326, an oral interleukin-12/23 inhibitor, in patients with active moderate to severe Crohn's disease. Inflamm. Bowel Dis. *12*, 558–565.

Cai, X., Xu, Y., Cheung, A.K., Tomlinson, R.C., Alcazar-Roman, A., Murphy, L., Billich, A., Zhang, B., Feng, Y., Klumpp, M., et al. (2013). PIKfyve, a class III PI kinase, is the target of the small molecular IL-12/IL-23 inhibitor apilimod and a

player in Toll-like receptor signaling. Chem. Biol. *20*, 912–921.

Cai, X., Xu, Y., Kim, Y.M., Loureiro, J., and Huang, Q. (2014). PIKfyve, a class III lipid kinase, is required for TLR-induced type I IFN production via modulation of ATF3. J. Immunol. *192*, 3383–3389.

Calafat, J., Nijenhuis, M., Janssen, H., Tulp, A., Dusseljee, S., Wubbolts, R., and Neefjes, J. (1994). Major histocompatibility complex class II molecules induce the formation of endocytic MIIC-like structures. J. Cell Biol. *126*, 967–977.

Castellino, F., and Germain, R.N. (1995). Extensive trafficking of MHC class II-invariant chain complexes in the endocytic pathway and appearance of peptide-loaded class II in multiple compartments. Immunity *2*, 73–88.

Compton, L.M., Ikonomov, O.C., Sbrissa, D., Garg, P., and Shisheva, A. (2016). Active vacuolar H+ ATPase and functional cycle of Rab5 are required for the vacuolation defect triggered by PtdIns(3,5)P2 loss under PIKfyve or Vps34 deficiency. Am. J. Physiol. Cell Physiol. *311*, C366–C377.

Currinn, H., Guscott, B., Balklava, Z., Rothnie, A., and Wassmer, T. (2016). APP controls the formation of PI(3,5)P(2) vesicles through its binding of the PIKfyve complex. Cellular and molecular life sciences. Cell. Mol. Life Sci. *73*, 393–408.

Dayam, R.M., Sun, C.X., Choy, C.H., Mancuso, G., Glogauer, M., and Botelho, R.J. (2017). The lipid kinase PIKfyve coordinates the neutrophil immune response through the activation of the Rac GTPase. J. Immunol. *199*, 2096–2105.

Denzin, L.K., Robbins, N.F., Carboy-Newcomb, C., and Cresswell, P. (1994). Assembly and intracellular transport of HLA-DM and correction of the class II antigen-processing defect in T2 cells. Immunity *1*, 595–606.

Dingjan, I., Linders, P.T., van den Bekerom, L., Baranov, M.V., Halder, P., Ter Beest, M., and van den Bogaart, G. (2017a). Oxidized phagosomal NOX2 complex is replenished from lysosomes. J. Cell Sci. *130*, 1285–1298.

Dingjan, I., Paardekooper, L.M., Verboogen, D.R.J., von Mollard, G.F., Ter Beest, M., and van den Bogaart, G. (2017b). VAMP8-mediated NOX2 recruitment to endosomes is necessary for antigen release. Eur. J. Cell Biol. *96*, 705–714.

Dingjan, I., Verboogen, D.R., Paardekooper, L.M., Revelo, N.H., Sittig, S.P., Visser, L.J., Mollard, G.F., Henriet, S.S., Figdor, C.G., Ter Beest, M., et al. (2016). Lipid peroxidation causes endosomal antigen release for cross-presentation. Sci. Rep. *6*, 22064.

Dong, X.P., Shen, D., Wang, X., Dawson, T., Li, X., Zhang, Q., Cheng, X., Zhang, Y., Weisman, L.S., Delling, M., et al. (2010). PI(3,5)P(2) controls membrane trafficking by direct activation of mucolipin Ca(2+) release channels in the endolysosome. Nat. Commun. *1*, 38.

Dove, S.K., Dong, K., Kobayashi, T., Williams, F.K., and Michell, R.H. (2009). Phosphatidylinositol 3,5-bisphosphate and Fab1p/PIKfyve underPPIn endo-lysosome function. Biochem. J. *419*, 1–13.

Egami, Y. (2016). Molecular imaging analysis of Rab GTPases in the regulation of phagocytosis and macropinocytosis. Anat. Sci. Int. *91*, 35–42.

Ellson, C.D., Anderson, K.E., Morgan, G., Chilvers, E.R., Lipp, P., Stephens, L.R., and Hawkins, P.T. (2001a). Phosphatidylinositol 3-phosphate is generated in phagosomal membranes. Curr. Biol. *11*, 1631–1635.

Ellson, C.D., Gobert-Gosse, S., Anderson, K.E., Davidson, K., Erdjument-Bromage, H., Tempst, P., Thuring, J.W., Cooper, M.A., Lim, Z.Y., Holmes, A.B., et al. (2001b). PtdIns(3)P regulates the neutrophil oxidase complex by binding to the PX domain of p40(phox). Nat. Cell Biol. *3*, 679–682.

Ewanchuk, B.W., and Yates, R.M. (2018). The phagosome and redox control of antigen processing. Free Rad. Biol. Med. *125*, 53–61.

Fairn, G.D., and Grinstein, S. (2012). How nascent phagosomes mature to become phagolysosomes. Trends Immunol. *33*, 397–405.

Flannagan, R.S., Cosio, G., and Grinstein, S. (2009). Antimicrobial mechanisms of phagocytes and bacterial evasion strategies. Nat. Rev. Microbiol. *7*, 355–366.

Flannagan, R.S., Jaumouille, V., and Grinstein, S. (2012). The cell biology of phagocytosis. Annu. Rev. Pathol. *7*, 61–98.

Fratti, R.A., Backer, J.M., Gruenberg, J., Corvera, S., and Deretic, V. (2001). Role of phosphatidylinositol 3-kinase and Rab5 effectors in phagosomal biogenesis and mycobacterial phagosome maturation arrest. J. Cell Biol. *154*, 631–644.

Gayle, S., Landrette, S., Beeharry, N., Conrad, C., Hernandez, M., Beckett, P., Ferguson, S.M., Mandelkern, T., Zheng, M., Xu, T., et al. (2017a). Identification of apilimod as a first-in-class PIKfyve kinase inhibitor for treatment of B-cell non-Hodgkin lymphoma. Blood *129*, 1768–1778.

Gayle, S., Landrette, S., Beeharry, N., Conrad, C., Hernandez, M., Beckett, P., Ferguson, S.M., Xu, T., Rothberg, J., and Lichenstein, H. (2017b). B-cell non-Hodgkin lymphoma: selective vulnerability to PIKFYVE inhibition. Autophagy *13*, 1082–1083.

Gillooly, D.J., Morrow, I.C., Lindsay, M., Gould, R., Bryant, N.J., Gaullier, J.M., Parton, R.G., and Stenmark, H. (2000). Localization of phosphatidylinositol 3-phosphate in yeast and mammalian cells. EMBO J. *19*, 4577–4588.

Gomez, N.M., Lu, W., Lim, J.C., Kiselyov, K., Campagno, K.E., Grishchuk, Y., Slaugenhaupt, S.A., Pfeffer, B.A., Fliesler, S.J., and Mitchell, C.H. (2018). Robust lysosomal calcium signaling through channel TRPML1 is impaired by lysosomal lipid accumulation. FASEB J. *32*, 782–794.

Groemping, Y., and Rittinger, K. (2005). Activation and assembly of the NADPH oxidase: a structural perspective. Biochem. J. *386*, 401–416.

Hari, A., Ganguly, A., Mu, L., Davis, S.P., Stenner, M.D., Lam, R., Munro, F., Namet, I., Alghamdi, E., Furstenhaupt, T., et al. (2015). Redirecting soluble antigen for MHC class I cross-presentation during phagocytosis. Eur. J. Immunol. *45*, 383–395.

Hay, J.C. (2007). Calcium: a fundamental regulator of intracellular membrane fusion? EMBO Rep. *8*, 236–240.

Hazeki, K., Nigorikawa, K., Takaba, Y., Segawa, T., Nukuda, A., Masuda, A., Ishikawa, Y., Kubota, K., Takasuga, S., and Hazeki, O. (2012). Essential roles of PIKfyve and PTEN on phagosomal phosphatidylinositol 3-phosphate dynamics. FEBS Lett. *586*, 4010–4015.

Ho, C.Y., Alghamdi, T.A., and Botelho, R.J. (2012). Phosphatidylinositol-3,5-bisphosphate: no longer the poor PIP2. Traffic *13*, 1–8.

Honey, K., and Rudensky, A.Y. (2003). Lysosomal cysteine proteases regulate antigen presentation. Nat. Rev. Immunol. *3*, 472–482.

Ikonomov, O.C., Sbrissa, D., and Shisheva, A. (2001). Mammalian cell morphology and endocytic membrane homeostasis require enzymatically active phosphoinositide 5-kinase PIKfyve. J. Biol. Chem. *276*, 26141–26147.

Ikonomov, O.C., Sbrissa, D., and Shisheva, A. (2009). YM201636, an inhibitor of retroviral budding and PIKfyve-catalyzed PtdIns(3,5)P2 synthesis, halts glucose entry by insulin in adipocytes. Biochem. Biophys. Res. Commun. *382*, 566–570.

Jancic, C., Savina, A., Wasmeier, C., Tolmachova, T., El-Benna, J., Dang, P.M., Pascolo, S., Gougerot-Pocidalo, M.A., Raposo, G., Seabra, M.C., et al. (2007). Rab27a regulates phagosomal pH and NADPH oxidase recruitment to dendritic cell phagosomes. Nat. Cell Biol. *9*, 367–378.

Jasanoff, A., Song, S., Dinner, A.R., Wagner, G., and Wiley, D.C. (1999). One of two unstructured domains of Ii becomes ordered in complexes with MHC class II molecules. Immunity *10*, 761–768.

Jefferies, H.B., Cooke, F.T., Jat, P., Boucheron, C., Koizumi, T., Hayakawa, M., Kaizawa, H., Ohishi, T., Workman, P., Waterfield, M.D., et al. (2008). A selective PIKfyve inhibitor blocks PtdIns(3,5)P(2) production and disrupts endomembrane transport and retroviral budding. EMBO Rep. *9*, 164–170.

Jensen, P.E. (1991). Reduction of disulfide bonds during antigen processing: evidence from a thiol-dependent insulin determinant. J. Exp. Med. *174*, 1121–1130.

Joffre, O.P., Segura, E., Savina, A., and Amigorena, S. (2012). Cross-presentation by dendritic cells. Nat. Rev. Immunol. *12*, 557–569.

Jones, P.P., Murphy, D.B., and McDevitt, H.O. (1978). Two-gene control of the expression of a murine Ia antigen. J. Exp. Med. *148*, 925–939.

Kanai, F., Liu, H., Field, S.J., Akbary, H., Matsuo, T., Brown, G.E., Cantley, L.C., and Yaffe, M.B. (2001). The PX domains of p47phox and p40phox bind to lipid products of PI(3)K. Nat. Cell Biol. *3*, 675–678.

Kerr, M.C., Wang, J.T., Castro, N.A., Hamilton, N.A., Town, L., Brown, D.L., Meunier, F.A., Brown, N.F., Stow, J.L., and Teasdale, R.D. (2010). Inhibition of the PtdIns(5) kinase PIKfyve disrupts intracellular replication of Salmonella. EMBO J. *29*, 1331–1347.

Kim, A., Hartman, I.Z., Poore, B., Boronina, T., Cole, R.N., Song, N., Ciudad, M.T., Caspi, R.R., Jaraquemada, D., and Sadegh-Nasseri, S. (2014a). Divergent paths for the selection of immunodominant epitopes from distinct antigenic sources. Nat. Commun. *5*, 5369.

Kim, G.H., Dayam, R.M., Prashar, A., Terebiznik, M., and Botelho, R.J. (2014b). PIKfyve inhibition interferes with phagosome and endosome maturation in macrophages. Traffic *15*, 1143–1163.

Kinchen, J.M., and Ravichandran, K.S. (2008). Phagosome maturation: going through the acid test. Nat. Rev. Mol. Cell Biol. *9*, 781–795.

Kirschke, H., Wiederanders, B., Bromme, D., and Rinne, A. (1989). Cathepsin S from bovine spleen. Purification, distribution, intracellular localization and action on proteins. Biochem. J. *264*, 467–473.

Kotsias, F., Hoffmann, E., Amigorena, S., and Savina, A. (2013). Reactive oxygen species production in the phagosome: impact on antigen presentation in dendritic cells. Antioxid. Redox Signal. *18*, 714–729.

Krausz, S., Boumans, M.J., Gerlag, D.M., Lufkin, J., van Kuijk, A.W., Bakker, A., de Boer, M., Lodde, B.M., Reedquist, K.A., Jacobson, E.W., et al. (2012). Brief report: a phase IIa, randomized, double-blind, placebo-controlled trial of apilimod mesylate, an interleukin-12/interleukin-23 inhibitor, in patients with rheumatoid arthritis. Arthritis Rheum. *64*, 1750–1755.

Krishna, S., Palm, W., Lee, Y., Yang, W., Bandyopadhyay, U., Xu, H., Florey, O., Thompson, C.B., and Overholtzer, M. (2016). PIKfyve regulates vacuole maturation and nutrient recovery following engulfment. Dev. Cell *38*, 536–547.

Levin, R., Grinstein, S., and Schlam, D. (2015). Phosphoinositides in phagocytosis and macropinocytosis. Biochim. Biophys. Acta *1851*, 805–823.

Li, S.C., Diakov, T.T., Xu, T., Tarsio, M., Zhu, W., Couoh-Cardel, S., Weisman, L.S., and Kane, P.M. (2014). The signaling lipid PI(3,5)P(2) stabilizes V(1)-V(o) sector interactions and activates the V-ATPase. Mol. Biol. Cell *25*, 1251–1262.

Li, X., Rydzewski, N., Hider, A., Zhang, X., Yang, J., Wang, W., Gao, Q., Cheng, X., and Xu, H. (2016). A molecular mechanism to regulate lysosome motility for lysosome positioning and tubulation. Nat. Cell Biol. *18*, 404–417.

Mantegazza, A.R., Savina, A., Vermeulen, M., Perez, L., Geffner, J., Hermine, O., Rosenzweig, S.D., Faure, F., and Amigorena, S. (2008). NADPH oxidase controls phagosomal pH and antigen cross-presentation in human dendritic cells. Blood *112*, 4712–4722.

McCartney, A.J., Zhang, Y., and Weisman, L.S. (2014). Phosphatidylinositol 3,5-bisphosphate: low abundance, high significance. Bioessays *36*, 52–64.

Min, S.H., Suzuki, A., Stalker, T.J., Zhao, L., Wang, Y., McKennan, C., Riese, M.J., Guzman, J.F., Zhang, S., Lian, L., et al. (2014). Loss of PIKfyve in platelets causes a lysosomal disease leading to inflammation and thrombosis in mice. Nat. Commun. *5*, 4691.

Na, H., Cho, M., and Chung, Y. (2016). Regulation of Th2 cell immunity by dendritic cells. Immune Netw. *16*, 1–12.

Nakagawa, T.Y., Brissette, W.H., Lira, P.D., Griffiths, R.J., Petrushova, N., Stock, J., McNeish, J.D., Eastman, S.E., Howard, E.D., Clarke, S.R., et al. (1999). Impaired invariant chain degradation and antigen presentation and diminished collagen-induced arthritis in cathepsin S null mice. Immunity *10*, 207–217.

Naufer, A., Hipolito, V.E.B., and Ganesan, S. (2018). pH of endophagosomes controls association of their membranes with Vps34 and PtdIns(3)P levels. J. Cell Biol. *217*, 329–346.

Neefjes, J., Jongsma, M.M.L., and Berlin, I. (2017). Stop or go? endosome positioning in the establishment of compartment architecture, dynamics, and function. Trends Cell Biol. *27*, 580–594.

Neefjes, J.J., and Ploegh, H.L. (1992). Inhibition of endosomal proteolytic activity by leupeptin blocks surface expression of MHC class II molecules and their conversion to SDS resistance alpha beta heterodimers in endosomes. EMBO J. *11*, 411–416.

Nunes, P., Demaurex, N., and Dinauer, M.C. (2013). Regulation of the NADPH oxidase and associated ion fluxes during phagocytosis. Traffic *14*, 1118–1131.

Oppelt, A., Haugsten, E.M., Zech, T., Danielsen, H.E., Sveen, A., Lobert, V.H., Skotheim, R.I., and Wesche, J. (2014). PIKfyve, MTMR3 and their product PtdIns5P regulate cancer cell migration and invasion through activation of Rac1. Biochem. J. *461*, 383–390.

Palmer, J.T., Rasnick, D., Klaus, J.L., and Bromme, D. (1995). Vinyl sulfones as mechanism-based cysteine protease inhibitors. J. Med. Chem. *38*, 3193–3196.

Pawlak, J.B., Gential, G.P., Ruckwardt, T.J., Bremmers, J.S., Meeuwenoord, N.J., Ossendorp, F.A., Overkleeft, H.S., Filippov, D.V., and van Kasteren, S.I. (2015). Bioorthogonal deprotection on the dendritic cell surface for chemical control of antigen cross-presentation. Angew. Chem. Int. Ed. *54*, 5628–5631.

Pawlak, J.B., Hos, B.J., van de Graaff, M.J., Megantari, O.A., Meeuwenoord, N., Overkleeft, H.S., Filippov, D.V., Ossendorp, F., and van Kasteren, S.I. (2016). The optimization of bioorthogonal epitope ligation within MHC-I complexes. ACS Chem. Biol. *11*, 3172–3178.

Riedl, J., Crevenna, A.H., Kessenbrock, K., Yu, J.H., Neukirchen, D., Bista, M., Bradke, F., Jenne, D., Holak, T.A., Werb, Z., et al. (2008). Lifeact: a versatile marker to visualize F-actin. Nat. Methods *5*, 605–607.

Riese, R.J., and Chapman, H.A. (2000). Cathepsins and compartmentalization in antigen presentation. Curr. Opin. Immunol. *12*, 107–113.

Riese, R.J., Mitchell, R.N., Villadangos, J.A., Shi, G.P., Palmer, J.T., Karp, E.R., De Sanctis, G.T., Ploegh, H.L., and Chapman, H.A. (1998). Cathepsin S activity regulates antigen presentation and immunity. J. Clin. Invest. *101*, 2351–2363.

Riese, R.J., Wolf, P.R., Bromme, D., Natkin, L.R., Villadangos, J.A., Ploegh, H.L., and Chapman, H.A. (1996). Essential role for cathepsin S in MHC class II-associated invariant chain processing and peptide loading. Immunity *4*, 357–366.

Rocha, N., and Neefjes, J. (2008). MHC class II molecules on the move for successful antigen presentation. EMBO J. *27*, 1–5.

Roche, P.A., and Furuta, K. (2015). The ins and outs of MHC class II-mediated antigen processing and presentation. Nat. Rev. Immunol. *15*, 203–216.

Rybicka, J.M., Balce, D.R., Chaudhuri, S., Allan, E.R., and Yates, R.M. (2012). Phagosomal proteolysis in dendritic cells is modulated by NADPH oxidase in a pH-independent manner. EMBO J. *31*, 932–944.

Rybicka, J.M., Balce, D.R., Khan, M.F., Krohn, R.M., and Yates, R.M. (2010). NADPH oxidase activity controls phagosomal proteolysis in macrophages through modulation of the lumenal redox environment of phagosomes. Proc. Natl. Acad. Sci. U S A *107*, 10496–10501.

Sadegh-Nasseri, S. (2016). A step-by-step overview of the dynamic process of epitope selection by major histocompatibility complex class II for presentation to helper T cells. F1000Res. *5*, 1305.

Sands, B.E., Jacobson, E.W., Sylwestrowicz, T., Younes, Z., Dryden, G., Fedorak, R., and Greenbloom, S. (2010). Randomized, double-blind, placebo-controlled trial of the oral interleukin-12/23 inhibitor apilimod mesylate for treatment of active Crohn's disease. Inflamm. Bowel Dis. *16*, 1209–1218.

Savina, A., Jancic, C., Hugues, S., Guermonprez, P., Vargas, P., Moura, I.C., Lennon-Dumenil, A.M., Seabra, M.C., Raposo, G., and Amigorena, S. (2006). NOX2 controls phagosomal pH to regulate antigen processing during crosspresentation by dendritic cells. Cell *126*, 205–218.

Sbrissa, D., Ikonomov, O.C., Filios, C., Delvecchio, K., and Shisheva, A. (2012). Functional dissociation between PIKfyve-synthesized PtdIns5P and PtdIns(3,5)P2 by means of the PIKfyve inhibitor YM201636. Am. J. Physiol. Cell Physiol. *303*, C436–C446.

Sbrissa, D., Ikonomov, O.C., Fu, Z., Ijuin, T., Gruenberg, J., Takenawa, T., and Shisheva, A. (2007). Core protein machinery for mammalian phosphatidylinositol 3,5-bisphosphate synthesis and turnover that regulates the progression of endosomal transport. Novel Sac phosphatase joins the ArPIKfyve-PIKfyve complex. J. Biol. Chem. *282*, 23878–23891.

Sbrissa, D., Ikonomov, O.C., and Shisheva, A. (2000). PIKfyve lipid kinase is a protein kinase: downregulation of 5′-phosphoinositide product formation by autophosphorylation. Biochemistry *39*, 15980–15989.

Sbrissa, D., Ikonomov, O.C., and Shisheva, A. (2002). Phosphatidylinositol 3-phosphate-interacting domains in PIKfyve. Binding specificity and role in PIKfyve. Endomenbrane localization. J. Biol. Chem. *277*, 6073–6079.

Sherer, N.M., Lehmann, M.J., Jimenez-Soto, L.F., Ingmundson, A., Horner, S.M., Cicchetti, G., Allen, P.G., Pypaert, M., Cunningham, J.M., and Mothes, W. (2003). Visualization of retroviral replication in living cells reveals budding into multivesicular bodies. Traffic *4*, 785–801.

Shi, G.P., Villadangos, J.A., Dranoff, G., Small, C., Gu, L., Haley, K.J., Riese, R., Ploegh, H.L., and Chapman, H.A. (1999). Cathepsin S required for normal MHC class II peptide loading and germinal center development. Immunity *10*, 197–206.

Shieh, P., Dien, V.T., Beahm, B.J., Castellano, J.M., Wyss-Coray, T., and Bertozzi, C.R. (2015). CalFluors: a universal motif for fluorogenic azide probes across the visible spectrum. J. Am. Chem. Soc. *137*, 7145–7151.

Shisheva, A. (2001). PIKfyve: the road to PtdIns 5-P and PtdIns 3,5-P(2). Cell Biol. Int. *25*, 1201–1206.

Shisheva, A., Sbrissa, D., and Ikonomov, O. (2015). Plentiful PtdIns5P from scanty PtdIns(3,5)P2 or from ample PtdIns? PIKfyve-dependent models: evidence and speculation (response to: DOI 10.1002/bies.201300012). Bioessays *37*, 267–277.

Steinman, R.M., and Nussenzweig, M.C. (2002). Avoiding horror autotoxicus: the importance of dendritic cells in peripheral T cell tolerance. Proc. Natl. Acad. Sci. U S A *99*, 351–358.

Stern, L.J., Brown, J.H., Jardetzky, T.S., Gorga, J.C., Urban, R.G., Strominger, J.L., and Wiley, D.C. (1994). Crystal structure of the human class II MHC protein HLA-DR1 complexed with an influenza virus peptide. Nature *368*, 215–221.

ten Broeke, T., Wubbolts, R., and Stoorvogel, W. (2013). MHC class II antigen presentation by dendritic cells regulated through endosomal sorting. Cold Spring Harb. Perspect. Biol. *5*, a016873.

Terajima, M., Kaneko-Kobayashi, Y., Nakamura, N., Yuri, M., Hiramoto, M., Naitou, M., Hattori, K., Yokota, H., Mizuhara, H., and Higashi, Y. (2016). Inhibition of c-Rel DNA binding is critical for the anti-inflammatory effects of novel PIKfyve inhibitor. Eur. J. Pharmacol. *780*, 93–105.

Teyton, L., O'Sullivan, D., Dickson, P.W., Lotteau, V., Sette, A., Fink, P., and Peterson, P.A. (1990). Invariant chain distinguishes between the exogenous and endogenous antigen presentation pathways. Nature *348*, 39–44.

Trombetta, E.S., Ebersold, M., Garrett, W., Pypaert, M., and Mellman, I. (2003). Activation of lysosomal function during dendritic cell maturation. Science *299*, 1400–1403.

Tulp, A., Verwoerd, D., Dobberstein, B., Ploegh, H.L., and Pieters, J. (1994). Isolation and characterization of the intracellular MHC class II compartment. Nature *369*, 120–126.

Turk, V., Stoka, V., Vasiljeva, O., Renko, M., Sun, T., Turk, B., and Turk, D. (2012). Cysteine cathepsins: from structure, function and regulation to new frontiers. Biochim. Biophys. Acta *1824*, 68–88.

Uribe-Querol, E., and Rosales, C. (2017). Control of phagocytosis by microbial pathogens. Front. Immunol. *8*, 1368.

Verdoes, M., Oresic Bender, K., Segal, E., van der Linden, W.A., Syed, S., Withana, N.P., Sanman, L.E., and Bogyo, M. (2013). Improved quenched fluorescent probe for imaging of cysteine cathepsin activity. J. Am. Chem. Soc. *135*, 14726–14730.

Verma, S., Dixit, R., and Pandey, K.C. (2016). Cysteine proteases: modes of activation and future prospects as pharmacological targets. Front. Pharmacol. *7*, 107.

Vieira, O.V., Bucci, C., Harrison, R.E., Trimble, W.S., Lanzetti, L., Gruenberg, J., Schreiber, A.D., Stahl, P.D., and Grinstein, S. (2003). Modulation of Rab5 and Rab7 recruitment to phagosomes by phosphatidylinositol 3-kinase. Mol. Cell. Biol. *23*, 2501–2514.

Villadangos, J.A., Driessen, C., Shi, G.P., Chapman, H.A., and Ploegh, H.L. (2000). Early endosomal maturation of MHC class II molecules independently of cysteine proteases and H-2DM. EMBO J. *19*, 882–891.

Villadangos, J.A., and Ploegh, H.L. (2000). Proteolysis in MHC class II antigen presentation: who's in charge? Immunity *12*, 233–239.

Vulcano, M., Dusi, S., Lissandrini, D., Badolato, R., Mazzi, P., Riboldi, E., Borroni, E., Calleri, A., Donini, M., Plebani, A., et al. (2004). Toll receptor-mediated regulation of NADPH oxidase in human dendritic cells. J. Immunol. *173*, 5749–5756.

Wada, Y., Cardinale, I., Khatcherian, A., Chu, J., Kantor, A.B., Gottlieb, A.B., Tatsuta, N., Jacobson, E., Barsoum, J., and Krueger, J.G. (2012). Apilimod inhibits the production of IL-12 and IL-23 and reduces dendritic cell infiltration in psoriasis. PLoS One *7*, e35069.

Wada, Y., Lu, R., Zhou, D., Chu, J., Przewloka, T., Zhang, S., Li, L., Wu, Y., Qin, J., Balasubramanyam, V., et al. (2007). Selective abrogation of Th1 response by STA-5326, a potent IL-12/IL-23 inhibitor. Blood *109*, 1156–1164.

West, M.A., Lucocq, J.M., and Watts, C. (1994). Antigen processing and class II MHC peptide-loading compartments in human B-lymphoblastoid cells. Nature *369*, 147–151.

Wong, C.O., Gregory, S., Hu, H., Chao, Y., Sepulveda, V.E., He, Y., Li-Kroeger, D., Goldman, W.E., Bellen, H.J., and Venkatachalam, K. (2017). Lysosomal degradation is required for sustained phagocytosis of bacteria by macrophages. Cell Host Microbe *21*, 719–730.e6.

Zavala-Ruiz, Z., Strug, I., Anderson, M.W., Gorski, J., and Stern, L.J. (2004). A polymorphic pocket at the P10 position contributes to peptide binding specificity in class II MHC proteins. Chem. Biol. *11*, 1395–1402.

Zwart, W., Griekspoor, A., Kuijl, C., Marsman, M., van Rheenen, J., Janssen, H., Calafat, J., van Ham, M., Janssen, L., van Lith, M., et al. (2005). Spatial separation of HLA-DM/HLA-DR interactions within MIIC and phagosome-induced immune escape. Immunity *22*, 221–233.

ISCI, Volume *11*

Supplemental Information

The Phosphoinositide Kinase PIKfyve Promotes Cathepsin-S-Mediated Major Histocompatibility Complex Class II Antigen Presentation

Maksim V. Baranov, Frans Bianchi, Anastasiya Schirmacher, Melissa A.C. van Aart, Sjors Maassen, Elke M. Muntjewerff, Ilse Dingjan, Martin ter Beest, Martijn Verdoes, Samantha G.L. Keyser, Carolyn R. Bertozzi, Ulf Diederichsen, and Geert van den Bogaart

SUPPLEMENTAL FIGURES

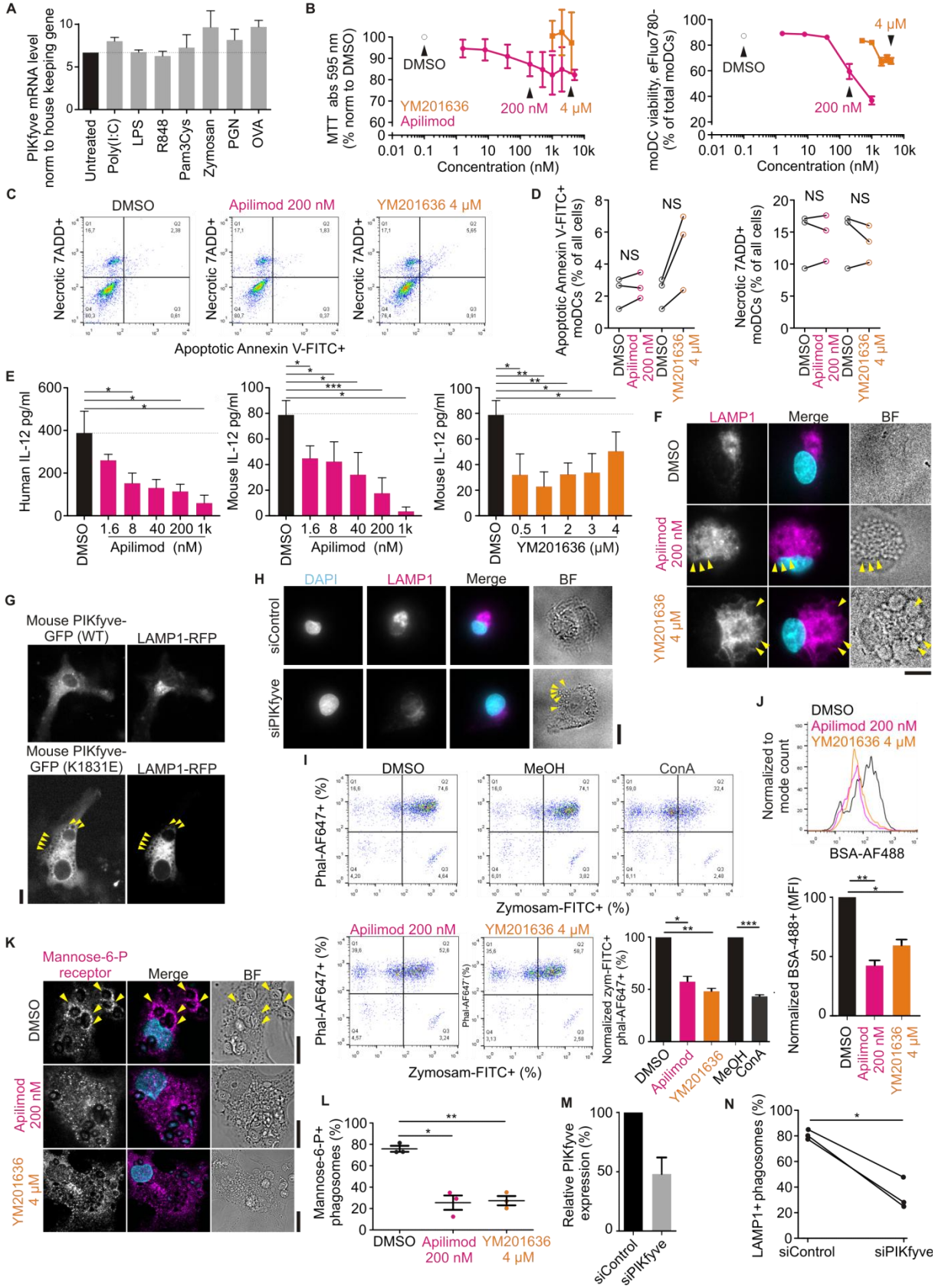

Figure S1. Characterization of PIKfyve inhibitors apilimod and YM201636. Related to Figure 2. (A) Expression of PIKfyve by qPCR in human monocyte-derived dendritic cells after 1 h stimulation with polyionosinic:polycytidylic acid (poly(I:C)) (TLR3 agonist); lipopolysaccharides (LPS) (TLR4 agonist);

resiquimod (R848) (TLR7 agonist); Pam(3)Cys (TLR2 agonist); zymosan (Dectin-1 and TLR2 agonist); pepdidoglycan (PGN) (TLR2 agonist); OVA (CD206 mannose receptor agonist). The expression levels were normalized to hydroxymethyl-bilane synthase (HMBS). (mean ± SEM for multiple donors). (B) Viability of human dendritic cells treated for 3 h with the indicated concentrations of apilimod or YM201636 by MTT assay (left) or fixable viability stain eFluo780 (right) (mean ± SEM for three donors). Black arrowheads: drug concentrations used throughout this study. DMSO: solvent control. (C) Representative flow cytometry dot-blots of dendritic cells stained with annexin-V (early apoptotic cells) and 7ADD (necrotic cells) after 3 h treatment with apilimod (200 nM) or YM201636 (4 µM). (D) Quantification of panel C (individual donors shown). Left panel: quantification of sum of Q2 and Q3 population of annexin-V positive early apoptotic cells. Right panel: quantification of populations in Q1 and Q2 of 7AAD-positive necrotic cells. NS: not significant. (E) IL-12 production measured after 24 h LPS (1 µg/ml) stimulation by human monocyte-derived dendritic cells (left) or murine bone-marrow-derived dendritic cells (middle and right) in the absence or presence of apilimod or YM201636 (mean ± SEM for three donors or mice). (F) Confocal images of monocyte-derived human dendritic cells treated with DMSO, apilimod or YM201636 and immunostained for LAMP1 (magenta in merge). Cyan: DAPI. BF: bright-field. Yellow arrowheads: enlarged vacuoles. (G) Confocal images of representative dendritic cells expressing LAMP1-RFP with mouse wild-type or kinase-dead (K1831E) PIKfyve-GFP. Yellow arrowheads: enlarged vacuoles with the kinase-dead PIKfyve-GFP. (H) Representative images of moDC with siRNA knockdown of PIKfyve (siPIKfyve). siControl: non-targeting siRNA control. Yellow arrowheads: enlarged vacuoles. BF: bright-field. (I) Phagocytosis by dendritic cells measured with flow cytometry and FITC-labeled zymosan particles (zymosan-FITC) and DMSO, apilimod or YM201636 treatment. Cells were labeled with phalloidin-Alexa Fluor 647 (phal-AF647). Bar graphs show quantification of phagocytosing cells (Q2 population in representative scatter plots; mean ± SEM of 3 donors). (J) Same as panel I, but now for endocytosis of BSA-Alexa Fluor 488 (BSA-AF488) for 1 h. Representative histograms shown. (K) Confocal images of zymosan-pulsed dendritic cells immunolabeled for mannose-6-phosphate receptor (magenta in merge) and with 3 h treatment with DMSO (solvent control), apilimod or YM201636. Yellow arrowheads: phagosomes positive for mannose-6-phosphate receptor. (L) Graph: quantification of panel G for 3 donors (~300 phagosomes/condition/donor; mean ± SEM). (M) Quantification of siPIKfyve by qPCR (mean ± SEM of 3 donors). (N) Quantification of LAMP1-positive phagosomes as in main Fig. 2A-D, but now with siPIKfyve. Zymosan was added for 1 h before fixation (~160 phagosomes/condition/donor). Scale bars: 10 µm.

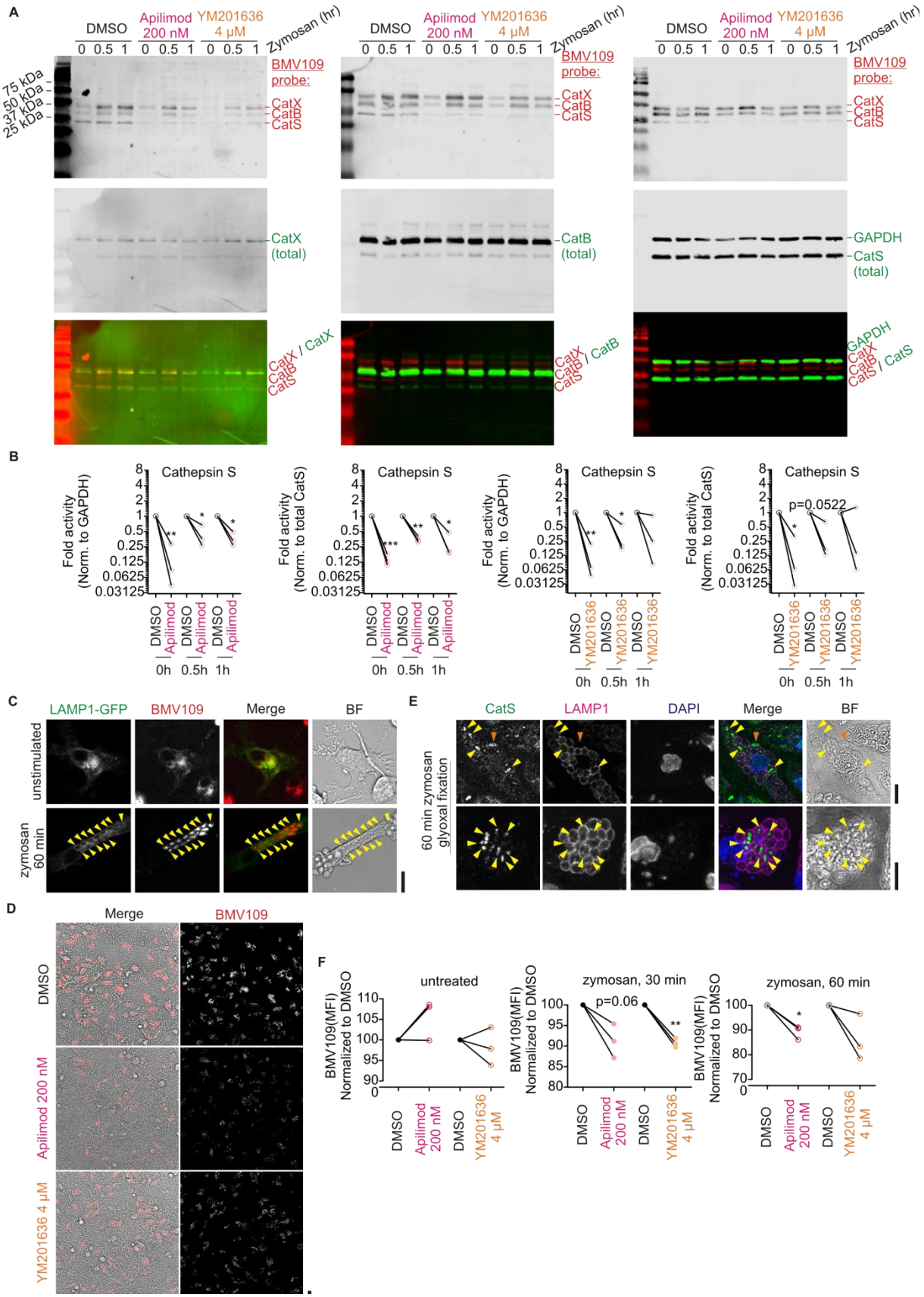

Figure S2. Control experiments for cathepsin activity and trafficking in human dendritic cells. Related to Figure 3. (A) Upper row: SDS-PAGE followed by in-gel fluorescence of human monocyte-derived dendritic cells treated with zymosan and activity-based probe BMV109-Cy5 (red bands in merge). Middle row:

subsequent immunoblotting to PVDF and labeling with antibodies specific for cathepsins (Cat) X, B and S and GAPDH (green bands in merge). Lower row: merged images of BMV109 probe (red) and immunolabeled cathepsins (green) or GAPDH (green, only labeled on the bottom right blot). Every column of images is from a separate donor. Full SDS PAGE/PVDF blots are shown. (B) Quantification of CatS activity measured from panel A. Normalization of each condition is either to GAPDH or total CatS (individual donors shown; normalized to DMSO controls). (C) Confocal live cell imaging of representative dendritic cells expressing GFP-tagged LAMP1 (LAMP1-GFP; green in merge) and pulsed with BMV109 (red in merge) after 1h of zymosan stimulation. Yellow arrowheads: phagosomes positive for LAMP1-GFP and BMV109 signal. BF: bright-field. (D) Representative confocal live cell image of dendritic cells treated as in panel A (1h with zymosan). (E) Confocal image of zymosan-pulsed dendritic cell with immunolabeling for LAMP1 (magenta in merge) and cathepsin S (green). Blue: DAPI. Yellow arrowheads: phagosomes positive for LAMP1 and CatS. Orange arrowhead: phagosome with CatS only. (F) Quantification of panel D (~500 images per condition/donor; mean ± SEM of 3 donors). Scale bars: 10 µm.

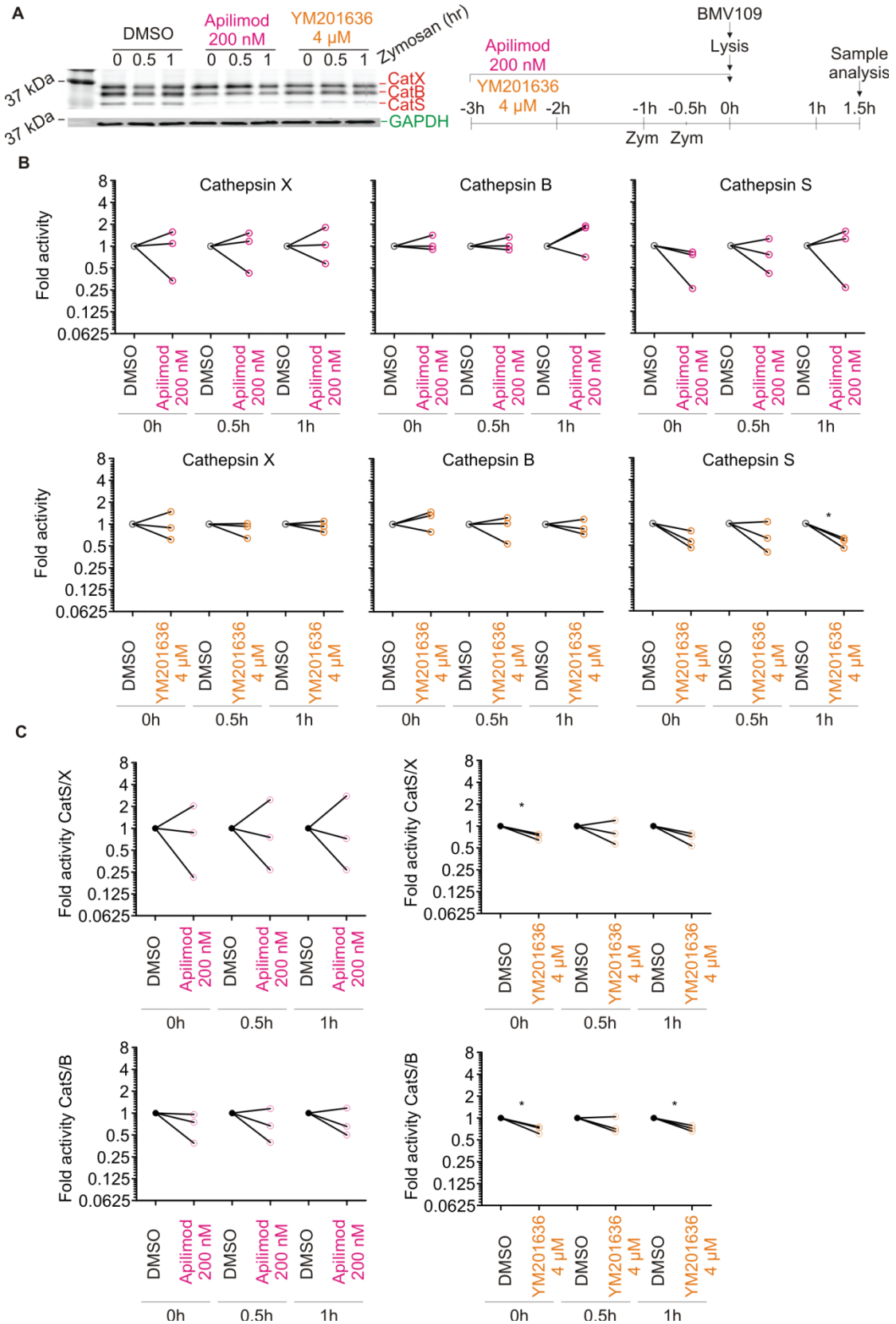

Figure S3. Cathepsin activity in lysate of human monocyte-derived dendritic cells. Related to Figure 3. (A) Zymosan pulsed dendritic cells were lysed and BMV109 probe was added to the cell lysates and incubated on ice for 1.5h. Lysates were resolved with SDS-PAGE and in-gel fluorescence (right-hand scheme). GAPDH: loading control by Western blot. Only part of the SDS PAGE/PVDF blot is shown, the rest of the image carried no information. (B) Quantification of BMV109 signals from panel A (3 donors; individual donors shown;

normalized to DMSO controls). (C) Same as panel B, but now BMV109 signal for CatS normalized to CatX and CatB.

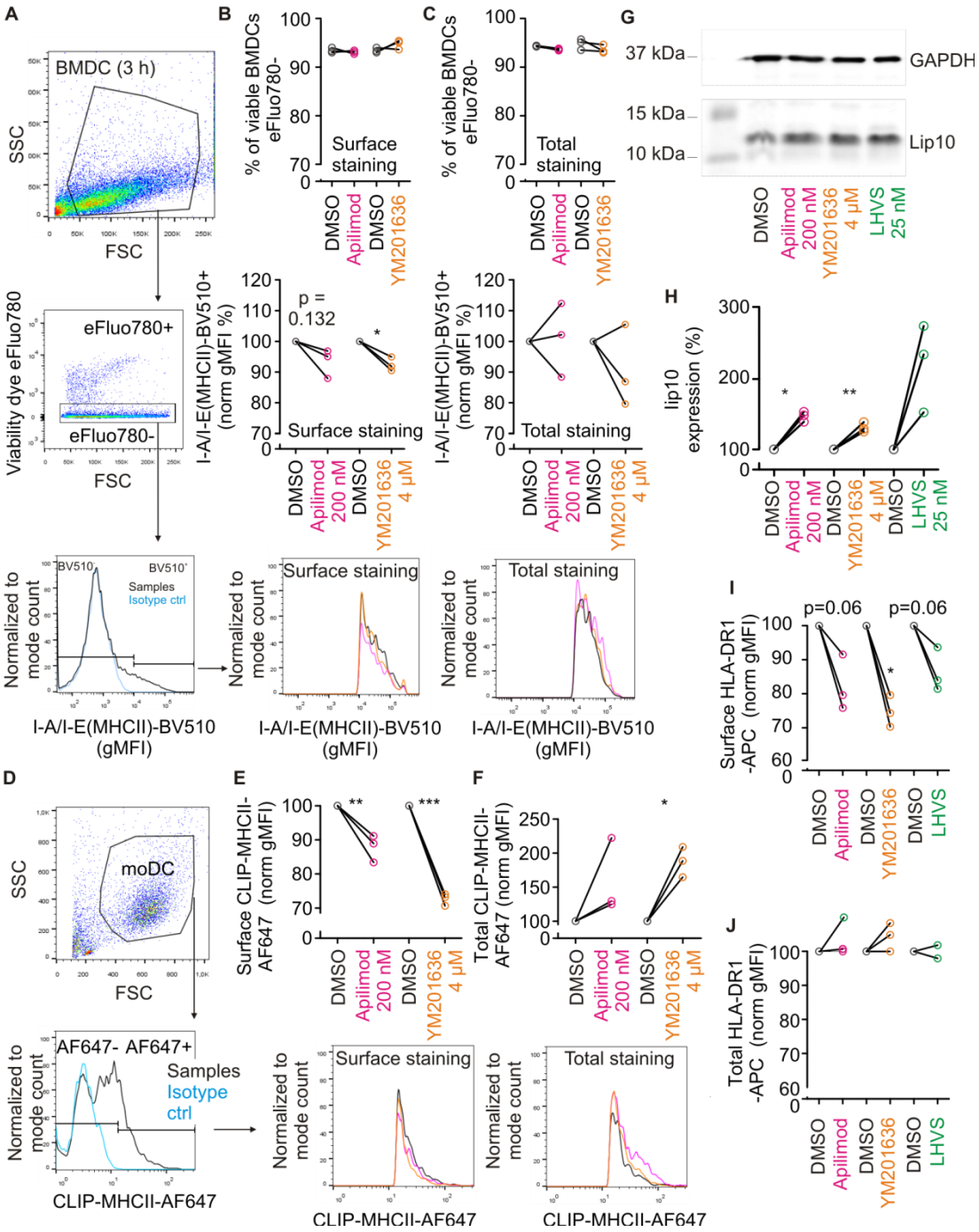

Figure S4. Control experiments for cathepsin activity and trafficking in human and mouse dendritic cells. Related to Figure 4. (A) Gating strategy for flow cytometry experiments with mouse bone-marrow derived dendritic cells (BMDCs) where surface MHC-II (I-A/I-E(MHCII)-BV510) was accessed in non-permeabilized cells negative for the fixable viability dye eFluo780. Representative histograms show the geometric mean fluorescence intensities (gMFI). Cells were treated for 3 h with apilimod or YM201636; SSC: side scatter. FSC: forward scatter. Light blue: isotype control. (B) Quantification of viable eFluo780-negative cells and surface MHC-II signals from panel A normalized to DMSO solvent controls (individual mice shown; normalized to DMSO controls). (C) Same as panels A-B, but now in presence of detergent permeabilization for assessment of total cellular MHC-II. (D) Gating strategy for flow cytometry of human monocyte-derived dendritic cells (moDC) immunolabeled using an antibody recognizing CLIP-bound MHC class II (CLIP-MHCII-AF647) labeled with Alexa Fluor-647 (AF647). (E) Representative histograms and quantification of surface CLIP-bound MHC class II (CLIP-MHCII-AF647) with flow cytometry experiments of moDCs treated for 3h with apilimod

(200 nM) or YM201636 (4 µM) (geometric mean fluorescence intensities (gMFI); individual donors shown; normalized to DMSO control). (F) Same as panel E, but now for total CLIP-bound MHC-II (Total CLIP-MHCII-AF647) with detergent permeabilization. (G) Representative Western blot of lysates from murine BMDCs labeled for CLIP. lip10: 10 kDa precursor fragment of CLIP. LHVS: selective cathepsin S inhibitor. GAPDH: loading control. Only part of the SDS PAGE/PVDF blot is shown, the rest of the image carried no information. (H) Quantification of panel G normalized to GAPDH (BMDCs from different mice shown; normalized to DMSO control). (I-J) Same as D-F, but now using an antibody recognizing MHC-II (HLA-DR1) conjugated with APC and an extra condition with CatS inhibitor LHVS (25 nM) (individual donors shown; normalized to DMSO controls).

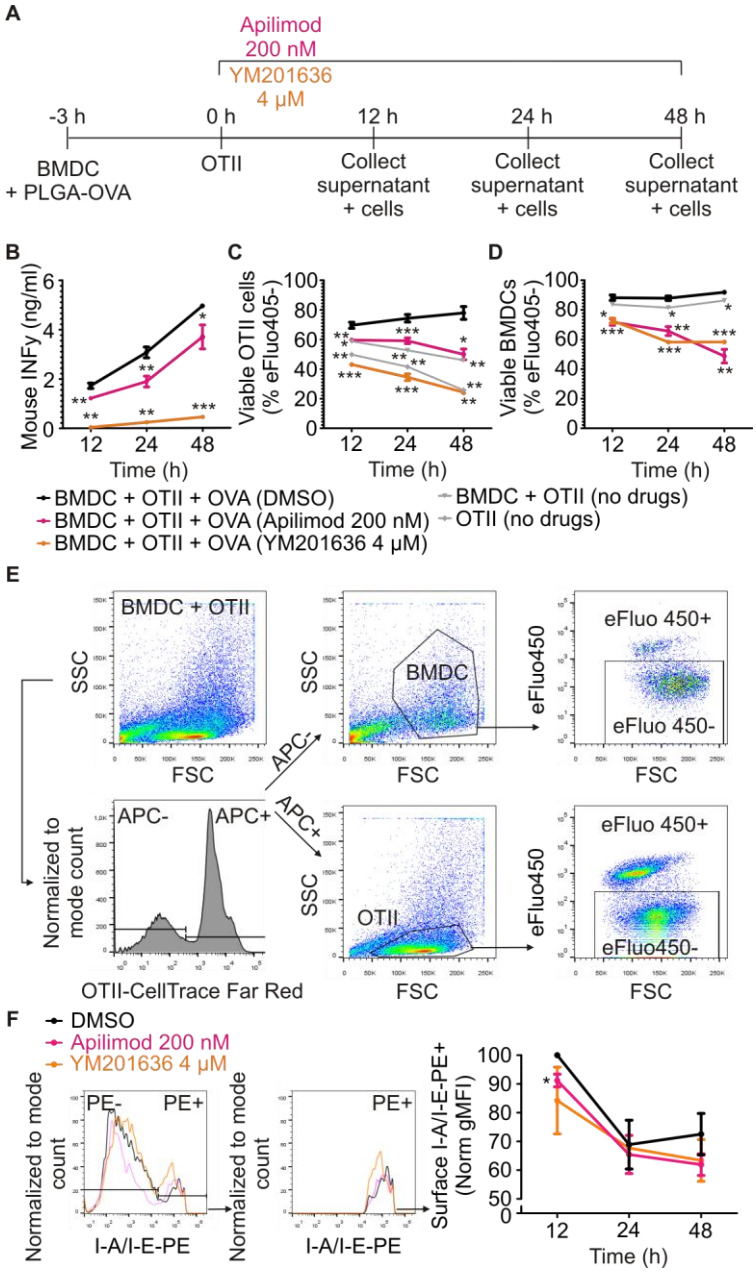

Figure S5. Control experiments for OT-II T cell priming experiments. Related to Figure 4. (A) Time line of murine OT-II T cell activation. Bone-marrow derived dendric cells (BMDC) were pre-incubated with PLGA-OVA particles for 3 hours. Subsequently, $OVA_{323-339}$-recognizing OT-II cells were added and the cells were exposed to apilimod or YM201636 for 12, 24 or 48 hours. (B) INFγ in supernatants by ELISA as indicated in panel A (mean from 3 independent experiments ± SEM). (C-E) Viability of experiment from panels A-B of OT-II cells (C) and BMDCs (D), and gating strategy (E). Viability was assessed with fixable viability dye eFluo405. OT-II cells were identified with OTII-CellTrace Far Red. SSC: side scatter; FSC: forward scatter (mean from 3 independent experiments ± SEM). (F) Surface expression of MHC class II (I-A/I-E-PE) for the experiments from panels A-E. gMFI: geometric mean fluorescence intensity. Representative histogram and quantifications are shown (normalized to DMSO control at 12 h; mean from 3 independent experiments ± SEM).

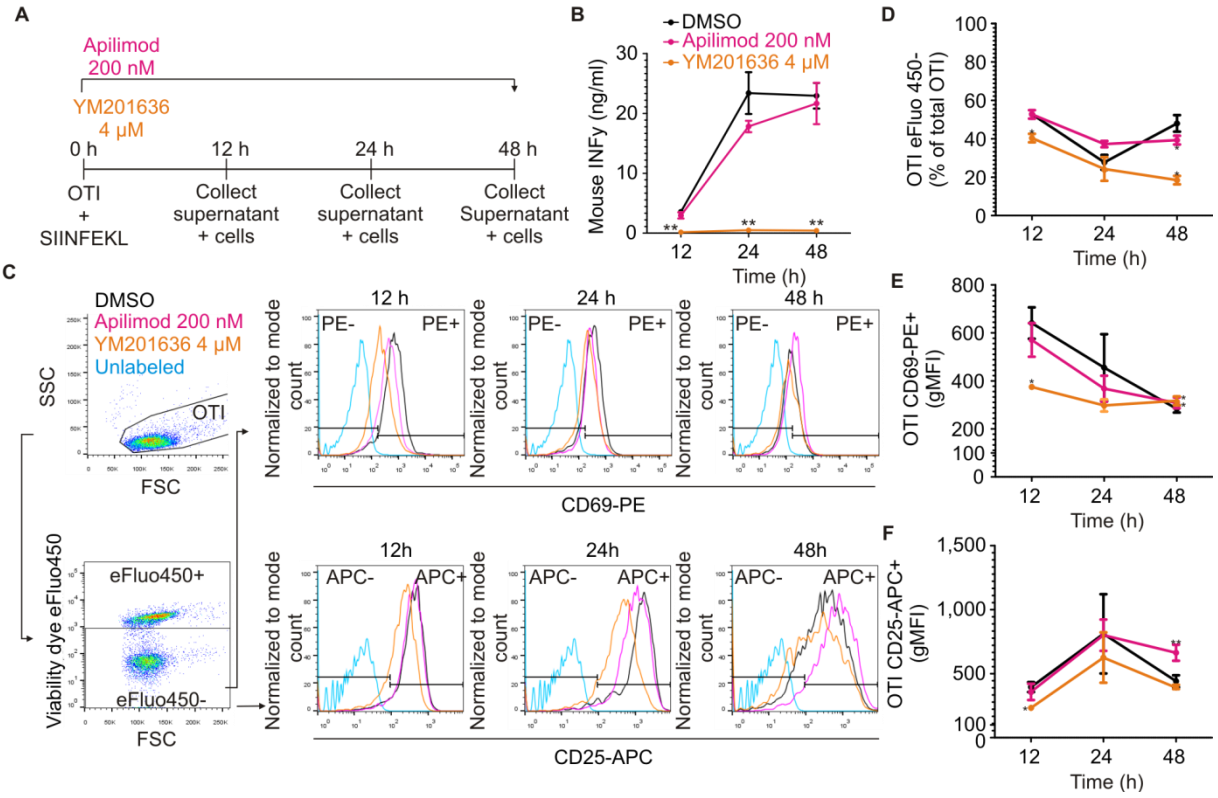

Figure S6. Apilimod and YM201636 impair T cell function. Related to Figure 4. (A) Scheme of experiment. OT-I T cells specifically recognizing ovalbumin residues 257-264 (SIINFEKL) in context of MHC-I were incubated with the epitope and PIKfyve inhibiting drugs apilimod or YM201636. (B) INFγ in the supernatants of the OT-I T cells from panel A. Note that YM201636 (but not or less apilimod) results in reduced production of INFγ. (C-F) Flow cytometry gating strategy and representative histograms (C) for T cell viability (D) and activation (E-F). Viability of OT-I T cells with fixable viability dye eFluo405 (D). Viable OT-I T cells were gated for early activation marker CD69-PE (E) or CD25-APC (F). SSC: side scatter; FSC: forward scatter; gMFI: geometric mean fluorescence intensity (mean from 3 independent experiments ± SEM).

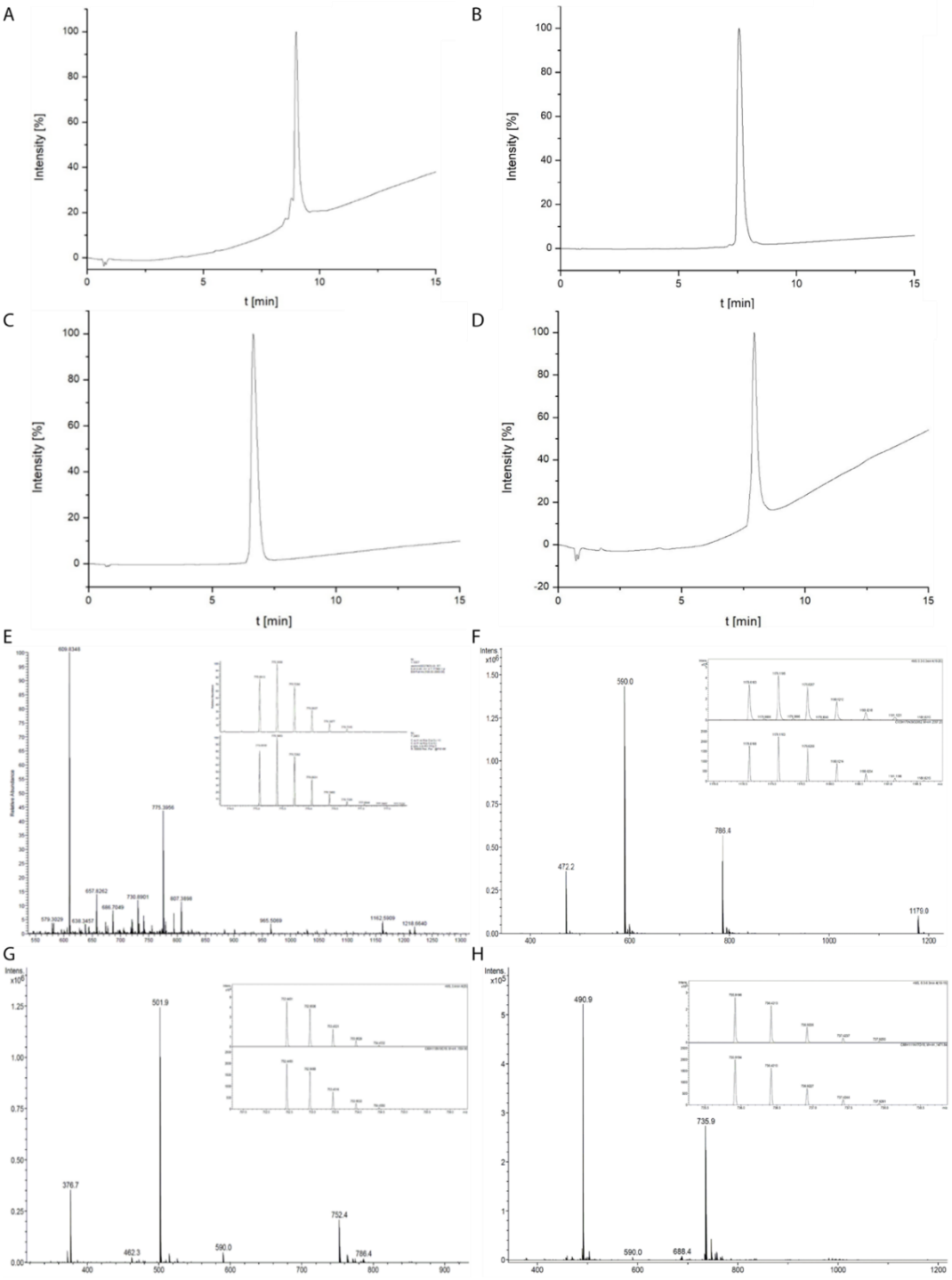

Figure S7. Analytical HPLC profiles and mass spectrometry validation of synthesized peptides. Related to Figure 6. Analytical HPLC chromatograms of: (A) hemagglutinin (HA) (residues 318-338) long clickable, (B) HA(318-338) long non clickable, (C) HA(322-334) short non clickable, and (D) HA(322-334) short clickable. ESI and HR-ESI-MS spectra of (E) HA(318-338) long clickable *m/z* (ESI) = 775.3956 $[M+3H]^{3+}$, 1162.5909 $[M+2H]^{2+}$ and *m/z* (HR-ESI-MS) = calculated: 775.0610 $[M+3H]^{3+}$, found: 775.0613 $[M+3H]^{3+}$, (F) HA(318-338) long non clickable *m/z* (ESI) = 472.2 $[M+5H]^{5+}$, 590.0 $[M+4H]^{4+}$, 786.4 $[M+3H]^{3+}$, 1079.0 $[M+2H]^{2+}$ and *m/z* (HR-ESI-MS) = calculated: 1178.6168 $[M+2H]^{2+}$, found: 1178.6183 $[M+2H]^{2+}$, (G) HA(322-334) short non clickable *m/z* (ESI) = 376.7 $[M+4H]^{4+}$, 501.9 $[M+3H]^{3+}$, 752.4 $[M+2H]^{2+}$ and *m/z* (HR-ESI-MS) = calculated: 752.4483 $[M+2H]^{2+}$, found: 752.4491 $[M+2H]^{2+}$ and (H) HA(322-334) short clickable *m/z* (ESI) = 490.9

$[M+3H]^{3+}$, 735.9 $[M+2H]^{2+}$ and *m/z* (HR-ESI-MS) = calculated: 735.9194 $[M+2H]^{2+}$, found: 735.9198 $[M+2H]^{2+}$.

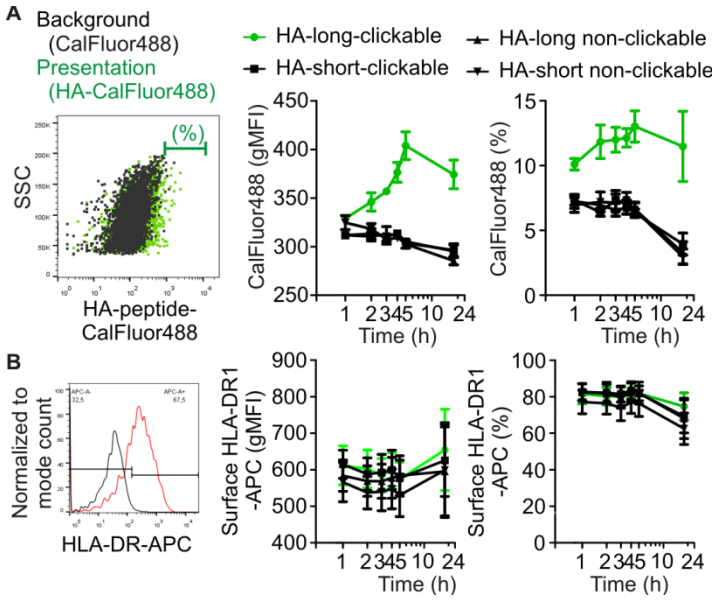

Figure S8. Control experiments for bio-orthogonal labeling of MHC-II presented epitope. Related to Figure 6. (A) Human dendritic cells were incubated with hemagglutinin (HA) peptides carrying an unnatural propargylglycine amino acid amendable to bio-orthoginal labeling with CalFluor488. Left: flow cytometry dot-blots with dendritic cells with (green) and without (background; black) HA peptide. SSC: side scatter. Right: gMFI (geometric mean fluorescence intensity) and population of HA-presenting cells incubated for the indicated times with long (residues 318-338) or short (residues 322-334) HA peptides with or without clickable propargylglycine amino acids. (B) The cells from panel A were tested for surface exposed MHC-II (HLA-DR) by flow cytometry. Representative histograms (left) and quantification by gMFI and population of HLA-DR-positive cells (right) are shown (mean from 5 donors ± SEM).

Table S1. Related to Figure 6. Synthesized hemagglutinin (HA) peptides with and without propargylglycine.

HA(318-338) long clickable	$C_{102}H_{163}N_{29}O_{29}S_2$ 2323.7 [g/mol]	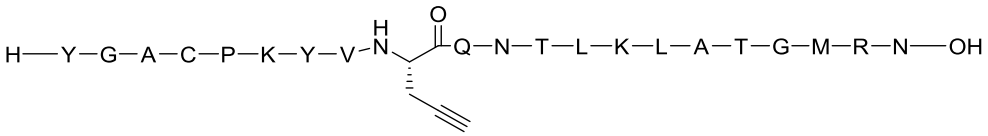
HA(318-338) long non clickable	$C_{103}H_{170}N_{30}O_{29}S_2$ 2356.8 [g/mol]	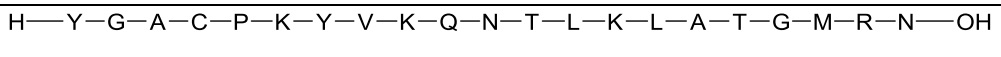
HA(322-334) short non clickable	$C_{69}H_{118}N_{18}O_{19}$ 1503.8 [g/mol]	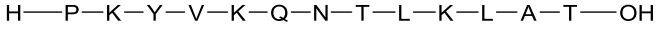
HA(322-334) short clickable	$C_{68}H_{111}N_{17}O_{19}$ 1469.8 [g/mol]	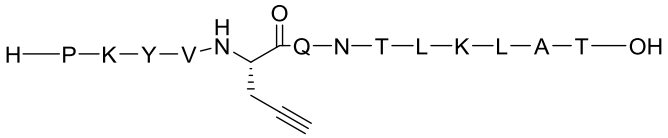

TRANSPARENT METHODS

Antibodies and reagents

The following antibodies were used: mouse monoclonal IgG1 anti-EEA1 at 1:100 (BD Biosciences; 610456 and 610457); rabbit polyclonal anti-LAMP-1 (CD107a) at 1:100 (Sigma; L1418); mouse monoclonal IgG1, κ anti-LAMP-1 (CD107a) at 1:100 (Biolegend; 328601, clone H4A3); mouse monoclonal IgG2a anti-M6PR at 1:50 in methanol fixed samples (Abcam; ab2733); rabbit polyclonal anti-GAPDH (14C10) at 1:1,000 (Cell Signaling; 2118); goat monoclonal IgG anti-Cathepsin X at 1:500 (R&D Systems; AF1033-SP); rabbit polyclonal anti-Cathepsin S at 1:250 (Novus Biologicals; NBP2-85807); mouse monoclonal IgG2a anti-Cathepsin B at 1:500 (Calbiochem; IM27L); mouse IgG2a,κ anti-HLA-DR, DP, DQ conjugated to FITC at 1:4 (BD Biosciences; clone Tü39) with isotype control mouse FITC-conjugated IgG2a,κ at 1:10 (BioLegend; 400208; clone MOPC-173); mouse monoclonal IgG1 anti-HLA-DR in complex with CLIP at 1:50 (Santa Cruz; sc-12725; clone CerCLIP.1); mouse IgG1, κ isotype control conjugated to APC at 1:10 (eBioscience; 17-4714-82); rat IgG2 anti-mouse CD74 at 1:500 (Biolegend; 151002); mouse monoclonal IgG1 anti-gp91^{phox} at 1:100 (D162-3; MBL); mouse anti-human-HLA-DR conjugated to APC at 1:100 (BD Biosciences; 559866; clone G46-6, RUO); mouse monoclonal IgG2a, κ anti-human-HLA-DR at 1:100 (Biolegend; 307614; clone L243); rat IgG2b,k anti-mouse I-A/I-E (MHC-II) conjugated to BV510 or PE at 1:200 (BioLegend; clone M5/114.15.2) with isotype control rat IgG2b,κ – BV510 or PE at 1:400 (Biolegend; 400645; clone RTK4530); anti-mouse CD69-PE from hamster at 1:100 (BD Biosciences; 553237; clone H1.2F3,RUO); anti-mouse CD25-APC from rat at 1:400 (eBioscience; 17-0251-82; clone PC61.5); OT-II were labeled with CellTrace Far Red labeling following the manufacturer's guidelines (ThermoFisher; C34564). The following secondary antibodies were used at (1:400): donkey-anti-mouse IgG (H&L) Alexa Fluor 647 (ThermoFisher; A-31571); donkey-anti-rabbit IgG (H&L) Alexa Fluor 568 (ThermoFisher; A-10042); goat-anti-mouse IgG (H&L) Alexa Fluor 488 (ThermoFisher; A-11029); goat-anti-Rabbit IgG (H + L) labeled with IRDye 800CW at 1:5,000 (LI-COR; 926-32211); goat-anti-rat Alexa Fluor 680 at 1:5,000 (ThermoFisher; A-21096).

Cell viability was assessed with the fixable viability dye eFluor450 (ThermoFisher; 65-0863-14) or eFluor780 (ThermoFisher; 65-0865-18) at 1:2,000 in PBS for 30 min on ice prior to 4% PFA fixation. The labeling for Flow cytometry was done as described (Baranov et al., 2016; Wimmers et al., 2016). All surface flow cytometry stainings were in PBA buffer (0.5% BSA and 0.01% NaN3 in PBS) and intracellular/total staining in PBA supplemented with 0.1% saponin as a detergent, all labeling was done for 10-30 min, PBS was used for washing. Annexin V-FITC (BD Biosciences;556419) and 7AAD (eBioscience; 00–6993–50) labeling was performed as described (Baranov et al., 2017) on ice for 10 min in buffer containing 1.5 mM $CaCl_2$. The MTT assay was performed as described (Baranov et al., 2016; Baranov et al., 2017) as follows: 0.66 mg/ml MTT (3-(4,5-dimethylthiazol-2-yl)-2,5-diphenyltetrazolium bromide; Sigma M2128-1G) was in contact with the cells for 2 h before lysis with the following buffer: 90% isopropanol, 0.0125% SDS and 0.04 M HCl. Absorbance was analyzed at 595 nm.

Apilimod (STA-5326) was from Axon Medchem (ID 1369; CAS 541550-19-0) and MT-Diagnostics (USbiol-002800) and was used at 200 nM. YM201636 was from Calbiochem (ID 524611; CAS 371942-69-7) and used at 4 µM. Phenylarsine oxide (PAO) (at 1 µM) was incubated for 1 hour as described (Dingjan et al., 2016). LHVS (at 25 nM) was used as selective inhibitor for cathepsin S (provided by Dr. M. Bogyo, Stanford School of Medicine, CA, USA) (Koblansky et al., 2013). For control conditions, 1% DMSO was used (*i.e.*, the highest vehicle content in all drug dilutions). In the cathepsin activity and confocal microscopy experiments, phagocytosis was induced using un-opsonized zymosan particles at a 1:10 and 1:5 cell-to-particle ratio respectively. For live cell microscopy, IgG-opsonized zymoson was used as described (Baranov et al., 2016). Briefly, 20 mg/ml zymosan suspension with an equal volume of opsonizing solution from ThermoFisher (Z2850) was incubated for 60 min at 37^{o}C and vigorously washed in PBS. BSA conjugated to Alexa fluor 488 was used at 10 µg/ml (ThermoFisher; A13100). Human IL12 was measured by ELISA using 96 flat bottom well plates (Microlon; 655092), coating antibody at 3 µg/ml (Pierce Endogen; M122), IL-12/IL-23 p40 detection antibody at 250 ng/ml (Thermo Scientific; M121B). Mouse IL12p70 (eBioscience; 88-7121-88) and INFγ (Invitrogen; 88-7314-88) were measured by ELISA following manufacturer's kit guidelines. All flow cytometry experiments were done on a FACS-Calibur cytometer or a FACS Verse system (both BD Bioscience).

Animals

OVA-T cell receptor transgenic OT-I mice purchased from Charles River Laboratories (Sherbrooke, PQ) and OT-II mice purchased from Jackson Laboratories (Bar Harbor, ME) were held in a pathogen-free environment in Nijmegen Central Animal Laboratory, Netherlands, in accordance with institutional and European guidelines and approved by the Animal Experimental Committee (Radboud UMC). CD8+ T cells recognizing $OVA_{257-264}$ SIINFEKL peptide or $CD4^+$ T cells recognizing $OVA_{323-339}$ peptide presented on H-$2IA^b$ MHC-II, were isolated from spleen as described (den Brok et al., 2016; Dolen et al., 2016).

MHC-II-restricted OVA presentation to OT-II

For BMDCs differentiation, bone marrow cells of 7-11 weeks old mice was isolated and cultured in RPMI 1640 medium (Gibco) (10% fetal calf serum (FCS), 1% L-alanyl-L-glutamine, 0.1% 2-Mercaptoethanol and 0.5% antibiotics/anti-mycotics (AA, Gibco)) supplemented with 20 ng/ml GM-CSF (Peprotech). BMDCs were collected between day 6-7 for experiments (Baranov et al., 2017). Poly(lactic-co-glycolic acid) (PLGA) particles containing OVA were prepared as described (Dolen et al., 2016) and 200 µg of particles containing 10 µg OVA were used to stimulate 50,000 GM-CSF-cultured day 6-7 mouse BMDCs in 100 µl per well (96 well plate) starvation serum-free RPMI (2.1 mM ultra-glutamine and 50 µM 2-Mercaptoethanol) for 3 hours before drug addition to ensure comparable OVA-PLGA uptake. Next, free OVA-PLGA particles were washed away and the medium was changed to 200 µl per well complete RPMI (10% FBS, 2.1 mM ultra-glutamine and 50 µM 2-Mercaptoethanol) containing 100,000 OT-II pre-labeled with CellTrace Far Red (DMSO, Apilimod and YM201636 were added in concentrations mentioned above). The supernatants for ELISA and cells for flow cytometry were collected at 12, 24 and 48 hours and the cells were immediately pretreated with viability dye eFluor on ice as mentioned above, then fixed and antibody-labeled for flow cytometry. OT-I cells were isolated from splenocytes as described (Baranov et al., 2017) from a 6 month old OT-I male mouse with a CD8a+ T Cell Isolation Kit (Miltenyi Biotec; 130–104–075) and directly stimulated with $OVA_{257-264}$ peptide (SIINFEKL) at 1 µg/ml.

Receptor stimulation, RNA isolation, cDNA synthesis and qPCR

For stimulation of pathogen recognition receptors the following ligands were used: polyionosinic:polycytidylic acid (Poly:IC)(TLR3 agonist) at 100 µg/ml for 4 hours; lipopolysaccharides (LPS) (TLR4 agonist) at 1 µg/ml for 4 hours; resiquimod (R848) (TLR7 agonist) at 2.5 µg/ml for 4 hours; Pam(3)Cys (TLR2 agonist) at 5 µg/ml for 4 hours; zymosan (Dectin-1 and TLR2 agonist) at $2x10^8$ particles/ml for 1 hour; pepdidoglycan (PGN) (LTR2 agonist) at 10 µg/ml for 1 hour; OVA (CD206 mannose receptor agonist) at 1 µg/ml for 1 h. After stimulation, RNA isolation was performed from 1 million dendritic cells using Quick-RNA MiniPrep kit (ZymoResearch) in accordance with the manufacturer's guidelines. For generating cDNA, master mix 1 (1 µl Random Hexamers (100 µM), 1.2 µl dNTPs (10 mM), RNA (1 µg) and H_2O) was made. This mix was incubated at 65°C for 5 minutes and directly chilled on ice. Mastermix 2 (4 µl 1st Buffer (5x), 2 µl DTT, 1µl RNAsin, 1 µl Reverse Transcriptase or H_2O) was added and the RT-program on a PCR machine was started. The RT-program consisted of the following steps: 10 min 25°C, 50 min 37°C, 15 min 70°C, pause at 4°C. After cDNA synthesis, qPCR was performed using 10 µl Sybr Green, 1.2 µl Primer Mix F + R (10 µM), 4.8 µl MQ and 4 µl cDNA (80 ng) dilution per well. The qPCR-program consisted of the following steps: 50°C for 2 minutes, 95°C for 10 minutes, 95°C for 15 seconds, 60 °C for 1 minute and repeated 39 times. The results were analyzed using the Bio-RAD Prime PCR program. The primers that were used for qPCR of PIKfyve were 5'-TGTCT GTGCT TGATC CAAGT G-3' and 5'-GCCAG GCCAA ATCAT CCTCT AA-3'.

siRNA knockdown assays

Post 72 hour knock-down in human dendritic cells was performed as described (Baranov et al., 2016). As control, siRNA irrelevant ON-TARGET plus non-targeting (NT) (Dharmacon) was used. The following cocktail of siRNAs was used for knockdown of PIKfyve (Invitrogen): 5'-GGAAA GGAAU UAGUC AACUG GCUAA-3', 5'-GGAGA CCUCC GAGCU UGCAC AUAUU-3', 5'-GAGGC CAGGG AGAAC AGCAG CCUUU-3'. Knockdown efficiency was measured with qPCR.

Microscopy and image processing

For the microscopy experiments, 100,000 dendritic cells were plated on 12 mm-diameter glass coverslips in serum free RPMI medium with 1% antibiotics/antimycotics and 2 mM ultra-glutamine and incubated at 37ºC and 5% CO_2. Fixation in most cases was done with 4% PFA solution in PBS. For CatS immunostaining, we performed antigen retrieval according to the manufacturer's protocol (R&D Systems; CTS013, CTS014, CTS015, CTS016). Fixation in 3% v/v glyoxal (Sigma-Aldrich #128465) for CatS and LAMP1 immunolabeling was done for 20 min as described (Richter and Revelo, 2018) and the solution mix was made with following ratios: 19.84 ml ddH_2O, 5.52 ml ethanol (absolute, for analysis), 2.18 ml glyoxal, 0.21 ml acetic acid, 1M NaOH was used to adjust pH to 4 or 5. Immunolabeling and blocking was performed with saponin permeabilization, as described (Baranov et al., 2016), in CLSM buffer (PBS with 20 mM glycine and 3% (w/v) BSA). Primary antibodies were incubated overnight, and secondary for 0,5-1h. In between, washing was done with PBS. Live cell imaging for BMV109 was done for 50,000 cells per well in µCLEAR F-bottom 96 well cell culture microplates (Greiner bio-one; 65500) in phenol red free and antibiotic free RPMI medium. The inhibitor and BMV109 concentrations and pipetting schemes were identical as for the in-gel fluorescence experiments. Samples were imaged with a Leica SP8 confocal laser scanning microscope with a 63x 1.20 NA water immersion objective (Leica HC PL APO 63x/1.20 W CORR CS2) or Leica DMI6000 epi-fluorescence microscope fitted with a 40× 0.85 NA dry objective, a metal halide EL6000 lamp for excitation, a DFC365FX CCD camera, and GFP and DsRed filter sets (all from Leica). Images were analyzed with Fiji (ImageJ).

Solid-phase peptide synthesis

Peptides were synthesized on a pre-loaded *Wang* resin (0.05 mmol, 0.27-0.32 mmol/g; Nova Biochem) on a Liberty Blue *CEM* microwave-assisted peptide synthesizer. The synthesis was conducted via a standard Fmoc/tBu-protocol using the recommended coupling (5 eq. amino acids, 5 eq. DIC, 5 eq. OxymaPure in DMF, 1: 75 °C, 170 W, 15 s, 2: 90 °C, 30 W, 50 s) and deprotection methods (piperidine/DMF, 1:4, *v/v*, 1: 75 °C, 155W, 15 s, 2: 90 °C, 30W, 50 s). The following L-amino acid building blocks were used in the automated synthesis: Fmoc-Ala-OH, Fmoc-Arg(Pbf)-OH, Fmoc-Asn(Trt)-OH, Fmoc-Cys(Trt)-OH, Fmoc-Gln(Trt)-OH, Fmoc-Gly-OH, Fmoc-Ile-OH, Fmoc-Leu-OH, Fmoc-Lys(Boc)-OH, Fmoc-Met-OH, Fmoc-Pro-OH, Fmoc-Thr(*t*Bu)-OH, Fmoc-Tyr(*t*Bu)-OH, Fmoc-Val-OH and Fmoc-Pra-OH (GL Biochem; ABCR). For all amino acids, except for arginine, single couplings were performed. Special care was taken for the incorporation of Cys, Pra and Arg residues. For cysteine and propargylglycine, the temperature of the microwave-assisted coupling was reduced and the reaction time elongated (1: 25 °C, 0 W, 120 s, 2: 50 °C, 30 W, 480 s). Arginine was introduced by double coupling ((a) 1: 25 °C, 0 W, 1500 s, 2: 75 °C, 30 W, 120 s, (b) 1: 75 °C, 30 W, 300 s). After synthesis, the resin was filtered off, washed successively with DMF (5 times), methanol (5 times) and DCM (10 times) and dried *in vacuo.* Acidic cleavage from the resin was achieved by treatment with a mixture of trifluoroacetic acid (TFA) / triisopropylsilane / ethanedithiol / water (94:2.5:2.5:1, 5 ml, 2 h). The resin was extracted with additional TFA (5 ml), and the combined extracts were concentrated to 2 ml under a flow of nitrogen. The crude peptide was then precipitated in cold diethylether (10 ml) and isolated by centrifugation and decantation of the supernatant. The precipitate was washed twice with ice-cold diethylether and subsequently dissolved in 5 mL of water and then freeze-dried to give a fine white solid.

Peptide purification

Peptides were purified by preparative reversed-phase HPLC using a Pharmacia Äcta Basic 900 device (pump type P-900, variable wavelength detector UV-900) at flow rates of 10 ml/min, and a Macherey-Nagel Nucleodur 100-5-C18 ec, (250 mm by 21 mm, 5 µm) reversed-phase column. Linear gradients of water and acetonitrile or methanol (solvent A: water, 0.1 % TFA, solvent B: acetonitrile / water 4:1, 0.1 % TFA or methanol, 0.1 % TFA) over 30 min were used for purification.

Peptide characterization

Peptides were characterized by electrospray ionisation (ESI) and high-resolution (HR-MS-ESI) mass spectrometry on a Bruker maXis spectrometer (Billerica, USA). Analytical HPLC measurements were

performed using a Thermo chromatography system (pumps UltiMate 3000, detector UltiMate 3000, autosampler UltiMate 3000 diode array) and an ACE Excel 2 C18 (2 µm, 2.1 x 100 mm) reversed-phase column at a flow rate of 0.4 ml/min. For peptide characterization, a linear gradient of water and methanol run (buffer A: water, 0.1 % TFA, buffer B: methanol, 0.85 % TFA) from 20-90 % buffer B over 15 min was used. Chromatograms were monitored at 220 nm wavelengths. The column was run at a controlled temperature of 50 °C.

Cell culture and transfection

Cultures of human monocyte-derived dendritic cells derived from peripheral blood monocytes (PBMCs) were obtained from buffy coats of healthy donors as described (Baranov et al., 2014; Baranov et al., 2016). Briefly, adherent monocytes isolated from the blood of healthy donors were in culture for 6 days in RPMI 1640 medium (Life Technologies) supplemented with 10% fetal bovine serum (FBS, Greiner Bio-one), 1 mM ultra-glutamine (BioWhittaker), antibiotics (100 U ml^{-1} penicillin, 100 µg ml^{-1} streptomycin and 0.25 µg ml^{-1} amphotericin B, Gibco), IL-4 (500 U ml^{-1}) and GM-CSF (800 U ml^{-1}). After that moDCs were detached from the plastic within 1h under cold PBS at $4^{O}C$ before freezing in liquid nitrogen in 10% DMSO and 40% FBS. Mouse GM-CSF differentiated BMDCs were generated as described (Baranov et al., 2017) and outlined above. The construct for full-length human PIKfyve was from Invivogen (cat nr puno1< hPIKFYVEb >) and subcloned in the EcoRI/BamHI sites of pEGFP-C1. pEGFP-HA-PIKfyve and pEGFP-HA-$PIKfyve^{K1831E}$ within pEGFP-C2 were obtained from Assia Shisheva (Ikonomov et al., 2001). LifeAct-RFP was a gift from Michael Sixt (Max Planck Institute of Biochemistry, Martinsried, Germany) (Riedl et al., 2008). The mRFP-tagged LAMP1 is described (Sherer et al., 2003) and LAMP1-mGFP was a gift from Esteban Dell'Angelica (Addgene plasmid # 34831 (Falcon-Perez et al., 2005)). NCF4-PX-EGFP was a gift from Michael Yaffe (Addgene plasmid #19010, (Kanai et al., 2001)). The YFP was replaced by mCherry in HLA-DRA-IRES-HLA-DRB-YFP, which was a gift from Jacques Neefjes (Netherlands Cancer Institute, Amsterdam, Netherlands) (Zwart et al., 2005). Transfection was performed as described (Baranov et al., 2014; Baranov et al., 2016) with a Neon Transfection system (Invitrogen), a ratio of 3 µg of DNA per $1*10^{6}$ cells was used, resuspended in 100 µl buffer R (Invitrogen) and electroporated (2 pulses of 40 ms, 1,000 V). After transfection, the cells were kept in antibiotic-free and serum-free RPMI medium (Invitrogen) for 3h before addition of full medium. Zymosan uptake and imaging experiments were performed 5–12 h post-transfection.

pHrodo zymosan

Dendritic cells (200,000 cells/well) were cultured in RPMI-1640 with 1% glutamine without phenol red in the presence of Apilimod or YM201636 for 3 h, in the final hour with drugs the cells were stimulated with 200 µl pHrodo Red Zymosan Bioparticles Conjugate for Phagocytosis (0.5 mg/ml) (ThermoFisher; P35364). Hoechst (5 µg/ml) was added 15 minutes before imaging. Samples were imaged with a Leica SP8 confocal laser scanning microscope with a 63x 1.20 NA water immersion objective (Leica HC PL APO 63x/1.20 W CORR CS2). Images were independently analyzed with Fiji (ImageJ) with identical treshholding parameters.

Cathepsin activity-based probe

Dendritic cells (300,000 cells/well) were cultured in RPMI-1640 with 1% ultra-glutamine (without Phenol Red) and incubated with different pharmacological treatments. Cells were stimulated using 15 µl unlabeled zymosan per well for 0, 0.5 or 1 h prior to lysis. Cathepsin probe BMV109-Cy5 at 1 µM (Verdoes et al., 2013) was added 0.5 h before lysis or in lysate control experiments probe BMV109-Cy5 was added immediately after lysis and incubated on ice for 1.5h. In lysate control experiments probe BMV109-Cy5 was added immediately after lysis. Cells were centrifuged and washed with ice-cold PBS, lysed in hypotonic lysis buffer (50 mM PIPES pH 7.4, 10 mM KCl, 5 mM $MgCl_2$, 2 mM EDTA, 4 mM DTT, and 1% NP-40). The cells were cooled on ice for 10 minutes. The lysates were transferred to new tubes and BCA protein determination was performed (Micro BCA™ Protein Assay Kit, Thermo Scientific; 23235). The samples were resolved on 15% SDS-PAGE and in-gel fluorescence of BMV109-Cy5 of active cathepsins was tested with a TRIO+ Typhoon scanner (670BP-500PMT-Rex-ex-Focal plane 3x). The SDS gel was subsequently blotted and immunostained for GAPDH loading control. The membrane was incubated with secondary antibody coupled with IRDye 680 or 800 at a dilution of 1:5,000 for 1

h. The membrane was washed three times with 0.05% Tween-20 for 10 minutes each and scanned with an Odyssey scanner (LI-COR). PAO was added to dendritic cells at 1 µM (Dingjan et al., 2016).

ROS measurements

ROS in apilimod treated dendritic cells was measured with the Amplex Red assay as described (Dingjan et al., 2016). Zymosan particles were co-labeled with ROS-sensor OxyBurst-Green H2DCFDA (ThermoFisher; D-2935) and Alexa-Fluor-633 C5-maleimide (A-20342, ThermoFisher) and live cell imaging was performed as described (Dingjan et al., 2017). For analysis, the OxyBurst fluorescence signal from each zymosan particle was divided by that of Alexa-Fluor-633.

HLA-DR1-restricted presentation of viral influenza HA

Peptides containing influenza A virus haemagglutin (strain A/Aichi/2/1968 H3N2) peptide (HA) residues 322-334 with or without lysine 326 converted into L-propargylglycine were synthesized (as described in ***Solid-phase peptide synthesis*** section). 100,000 dendritic cells were pre-stimulated for 5 h in 100 µl serum-free RPMI with a water solution of HA-peptide at 5 µM final concentration. Apilimod or YM201636 were added 3 h prior to the end of the HA-stimulation. As a control, cells were incubated for 15 min at 37^{o}C with trypsin-containing buffer (NaCl 0.8% (w/v), KCl 0.04% (w/v), D-glucose 0.1% (w/v), $NaHCO_3$ 0.058% (w/v), EDTA 0.02% (w/v), trypsin 0.05% (w/v) (BD Difco 250; 215240)). Cell viability was traced with eFluor780 (ThermoFisher; 65-0865-18) and cells were fixed in 4% PFA in PBS. At all steps before and during viability staining or click-labeling, the cells were washed at least 2 times with either PBS or HBS (N_2-bubbled, NaCl 150 mM, HEPES 20 mM, pH 7.4). Autofluorescence was reduced after 20 min by washing with quenching buffer (100 mM glycine, 100 mM NH_4Cl), surface presentation of HA was labeled for 1 h with CalFluor488 (Shieh et al., 2015) in HBS containing 1 mM $CuSO_4$, 0.5 mM THPTA (Tris(3-hydroxypropyltriazolylmethyl)amine), 5 mM sodium L-ascorbate; 0.01% (w/v) BSA, aminoguanidine 2.2% (w/v). Finally, surface HLA-DR1 was labeled with mouse anti-human-HLA-DR conjugated to APC at 1:100 (BD Biosciences; 559866; clone G46-6, RUO) in PBA buffer (0.5% BSA and 0.01% NaN_3 in PBS).

Statistical Analysis

All data were analyzed using Student's two-tailed paired t tests. A p value < 0.05 was regarded as statistically significant ($*p < 0.05$, $**p < 0.01$, $***p < 0.001$).

SUPPLEMENTAL REFERENCES

Baranov, M., Ter Beest, M., Reinieren-Beeren, I., Cambi, A., Figdor, C.G., and van den Bogaart, G. (2014). Podosomes of dendritic cells facilitate antigen sampling. Journal of cell science *127*, 1052-1064.

den Brok, M.H., Bull, C., Wassink, M., de Graaf, A.M., Wagenaars, J.A., Minderman, M., Thakur, M., Amigorena, S., Rijke, E.O., Schrier, C.C., *et al.* (2016). Saponin-based adjuvants induce cross-presentation in dendritic cells by intracellular lipid body formation. Nature communications *7*, 13324.

Dolen, Y., Kreutz, M., Gileadi, U., Tel, J., Vasaturo, A., van Dinther, E.A., van Hout-Kuijer, M.A., Cerundolo, V., and Figdor, C.G. (2016). Co-delivery of PLGA encapsulated invariant NKT cell agonist with antigenic protein induce strong T cell-mediated antitumor immune responses. Oncoimmunology *5*, e1068493.

Falcon-Perez, J.M., Nazarian, R., Sabatti, C., and Dell'Angelica, E.C. (2005). Distribution and dynamics of Lamp1-containing endocytic organelles in fibroblasts deficient in BLOC-3. Journal of cell science *118*, 5243-5255.

Koblansky, A.A., Jankovic, D., Oh, H., Hieny, S., Sungnak, W., Mathur, R., Hayden, M.S., Akira, S., Sher, A., and Ghosh, S. (2013). Recognition of profilin by Toll-like receptor 12 is critical for host resistance to Toxoplasma gondii. Immunity *38*, 119-130.

Richter, K.N., and Revelo, N.H. (2018). Glyoxal as an alternative fixative to formaldehyde in immunostaining and super-resolution microscopy. *37*, 139-159.

Wimmers, F., Aarntzen, E.H., Duiveman-deBoer, T., Figdor, C.G., Jacobs, J.F., Tel, J., and de Vries, I.J. (2016). Long-lasting multifunctional CD8(+) T cell responses in end-stage melanoma patients can be induced by dendritic cell vaccination. Oncoimmunology *5*, e1067745.